



# Novel Materials, Processing, and Device Technologies for Space Exploration With Potential Dual-Use Applications

*A.F. Hepp, S.G. Bailey, and J.S. McNatt  
Glenn Research Center, Cleveland, Ohio*

*M.V.S. Chandrashekar  
University of South Carolina, Columbia, South Carolina*

*J.D. Harris, A.W. Rusch, K.A. Nogales, K.V. Goettsche, and W. Hanson  
Northwest Nazarene University, Nampa, Indiana*

*D. Amos, V.K. Vendra, and C. Woodbury  
University of Louisville, Louisville, Kentucky*

*P. Hari and K.P. Roberts  
Nanotechnology Institute, University of Tulsa, Tulsa, Oklahoma*

*A.D. Jones, Jr.  
Florida Agricultural and Mechanical University, Tallahassee, Florida*

## NASA STI Program . . . in Profile

Since its founding, NASA has been dedicated to the advancement of aeronautics and space science. The NASA Scientific and Technical Information (STI) Program plays a key part in helping NASA maintain this important role.

The NASA STI Program operates under the auspices of the Agency Chief Information Officer. It collects, organizes, provides for archiving, and disseminates NASA's STI. The NASA STI Program provides access to the NASA Technical Report Server—Registered (NTRS Reg) and NASA Technical Report Server—Public (NTRS) thus providing one of the largest collections of aeronautical and space science STI in the world. Results are published in both non-NASA channels and by NASA in the NASA STI Report Series, which includes the following report types:

- TECHNICAL PUBLICATION. Reports of completed research or a major significant phase of research that present the results of NASA programs and include extensive data or theoretical analysis. Includes compilations of significant scientific and technical data and information deemed to be of continuing reference value. NASA counter-part of peer-reviewed formal professional papers, but has less stringent limitations on manuscript length and extent of graphic presentations.
- TECHNICAL MEMORANDUM. Scientific and technical findings that are preliminary or of specialized interest, e.g., “quick-release” reports, working papers, and bibliographies that contain minimal annotation. Does not contain extensive analysis.
- CONTRACTOR REPORT. Scientific and technical findings by NASA-sponsored contractors and grantees.
- CONFERENCE PUBLICATION. Collected papers from scientific and technical conferences, symposia, seminars, or other meetings sponsored or co-sponsored by NASA.
- SPECIAL PUBLICATION. Scientific, technical, or historical information from NASA programs, projects, and missions, often concerned with subjects having substantial public interest.
- TECHNICAL TRANSLATION. English-language translations of foreign scientific and technical material pertinent to NASA's mission.

For more information about the NASA STI program, see the following:

- Access the NASA STI program home page at <http://www.sti.nasa.gov>
- E-mail your question to [help@sti.nasa.gov](mailto:help@sti.nasa.gov)
- Fax your question to the NASA STI Information Desk at 757-864-6500
- Telephone the NASA STI Information Desk at 757-864-9658
- Write to:  
NASA STI Program  
Mail Stop 148  
NASA Langley Research Center  
Hampton, VA 23681-2199



# Novel Materials, Processing, and Device Technologies for Space Exploration With Potential Dual-Use Applications

*A.F. Hepp, S.G. Bailey, and J.S. McNatt  
Glenn Research Center, Cleveland, Ohio*

*M.V.S. Chandrashekar  
University of South Carolina, Columbia, South Carolina*

*J.D. Harris, A.W. Rusch, K.A. Nogales, K.V. Goettsche, and W. Hanson  
Northwest Nazarene University, Nampa, Indiana*

*D. Amos, V.K. Vendra, and C. Woodbury  
University of Louisville, Louisville, Kentucky*

*P. Hari and K.P. Roberts  
Nanotechnology Institute, University of Tulsa, Tulsa, Oklahoma*

*A.D. Jones, Jr.  
Florida Agricultural and Mechanical University, Tallahassee, Florida*

Prepared for  
Propulsion and Energy Forum 2014  
sponsored by the American Institute of Aeronautics and Astronautics  
Cleveland, Ohio, July 28–30, 2014

National Aeronautics and  
Space Administration

Glenn Research Center  
Cleveland, Ohio 44135

## Acknowledgments

NASA Glenn Research Center (GRC) is acknowledged for financial support of the work described in this paper, we thank Dr. Dennis Flood for his and support. We acknowledge the contributions of our colleagues: Dr. Geoff Landis, GRC; Drs. Castro, Banger, and Jin of Ohio Aerospace Institute; Phil Jenkins and Dave Scheiman, Naval Research Laboratory; Dr. Jon Cowen, Case Western Reserve University; Prof. Andy Barron, Rice University; and Prof. Ryne Raffaele at Rochester Institute of Technology. Several of us (Profs. Amos, Hari, and Harris) thank the NASA Experimental Program to Stimulate Competitive Research (EPSCoR) program for funding. Prof. M.V.S. Chandrashekar acknowledges the National Science Foundation (NSF), Office of Naval Research, and Department of Energy for financial support. Prof. J.D. Harris gratefully acknowledges financial support from the NSF through grant DMR 0840265 and A. Punnoose and J. Brotherton, P. Walker and W.B. Knowlton at Boise State University for their assistance. Prof. Andrew Jones acknowledges the Nuclear Regulatory Commission for financial support.

This report contains preliminary findings,  
subject to revision as analysis proceeds.

Trade names and trademarks are used in this report for identification  
only. Their usage does not constitute an official endorsement,  
either expressed or implied, by the National Aeronautics and  
Space Administration.

*Level of Review:* This material has been technically reviewed by technical management.

Available from

NASA STI Program  
Mail Stop 148  
NASA Langley Research Center  
Hampton, VA 23681-2199

National Technical Information Service  
5285 Port Royal Road  
Springfield, VA 22161  
703-605-6000

This report is available in electronic form at <http://www.sti.nasa.gov/> and <http://ntrs.nasa.gov/>

# Novel Materials, Processing, and Device Technologies for Space Exploration With Potential Dual-Use Applications

A.F. Hepp, S.G. Bailey, and J.S. McNatt  
National Aeronautics and Space Administration  
Glenn Research Center  
Cleveland, Ohio 44135

M.V.S. Chandrashekar  
University of South Carolina  
Columbia, South Carolina 29208

J.D. Harris, A.W. Rusch, K.A. Nogales, K.V. Goettsche, and W. Hanson  
Northwest Nazarene University  
Nampa, Indiana 83686

D. Amos, V.K. Vendra, and C. Woodbury  
University of Louisville  
Louisville, Kentucky 40292

P. Hari and K.P. Roberts  
Nanotechnology Institute  
University of Tulsa  
Tulsa, Oklahoma 74104

A.D. Jones, Jr.  
Florida Agricultural and Mechanical University  
Tallahassee, Florida 32301

## Abstract

We highlight results of a broad spectrum of efforts on lower-temperature processing of nanomaterials, novel approaches to energy conversion, and environmentally rugged devices. Solution-processed quantum dots of copper indium chalcogenide semiconductors and multiwalled carbon nanotubes from lower-temperature spray pyrolysis are enabled by novel (precursor) chemistry. Metal-doped zinc oxide (ZnO) nanostructured components of photovoltaic cells have been grown in solution at low temperature on a conductive indium tin oxide substrate. Arrays of ZnO nanorods can be templated and decorated with various semiconductor and metallic nanoparticles. Utilizing ZnO in a more broadly defined energy conversion sense as photocatalysts, unwanted organic waste materials can potentially be repurposed. Current efforts on charge carrier dynamics in nanoscale electrode architectures used in photoelectrochemical cells for generating solar electricity and fuels are described. The objective is to develop oxide nanowire-based electrode architectures that exhibit improved charge separation, charge collection and allow for efficient light absorption. Investigation of the charge carrier transport and recombination properties of the electrodes will aid in the understanding of how nanowire architectures improve performance of electrodes for dye-sensitized

solar cells. Nanomaterials can be incorporated in a number of advanced higher-performance (i.e., mass specific power) photovoltaic arrays. Advanced technologies for the deposition of 4H-silicon carbide are described. The use of novel precursors, advanced processing, and process studies, including modeling are discussed from the perspective of enhancing the performance of this promising material for enabling technologies such as solar electric propulsion.

## Nomenclature

|                       |                                                                      |
|-----------------------|----------------------------------------------------------------------|
| AAO                   | anodized aluminum oxide                                              |
| AM0                   | air mass zero (space solar spectrum)                                 |
| CBD                   | chemical bath deposition                                             |
| CNT                   | carbon nanotube                                                      |
| CuInS(e) <sub>2</sub> | copper indium disulf(selen)ide                                       |
| DFT                   | density functional theory                                            |
| DGM                   | dusty gas model; mathematical model of gas transport in porous media |
| DSSC                  | dye-sensitized solar cell                                            |
| E <sub>g</sub>        | bandgap energy                                                       |
| FTO                   | fluorin-doped tin oxide                                              |
| HR-TEM                | high resolution-transmission electron microscopy                     |
| HW-CVD                | hot wall-chemical vapor deposition                                   |

|                  |                                                                                        |
|------------------|----------------------------------------------------------------------------------------|
| IMPS             | integrated microelectronic power supply                                                |
| LEO              | low Earth orbit                                                                        |
| MWNT             | multiwall (carbon) nanotube                                                            |
| SEM              | scanning electron microscopy                                                           |
| SEP              | solar electric propulsion                                                              |
| SiC              | silicon carbide; wide-bandgap semiconductor (cubic (3C) and hexagonal (4H) polymorphs) |
| TEMPO            | (2,2,6,6-tetramethylpiperidin-1-yl)oxy                                                 |
| TiO <sub>2</sub> | titanium dioxide; typically found in either anatase or rutile phases                   |
| TOPO             | trioctylphosphine oxide                                                                |
| XRD              | x-ray diffraction                                                                      |
| ZnO              | zinc oxide; a wide-bandgap semiconductor                                               |

## 1.0 Introduction and Background

Ready and reliable power is an essential cornerstone of any successful space exploration venture—both manned and robotic. Solar array designs have undergone a steady evolution since the Vanguard 1 satellite. Early satellites used silicon solar cells on honeycomb panels that were body mounted to the spacecraft; early space solar arrays only produced a few hundred watts of power. Satellites today require low-mass solar arrays that produce several kilowatts of power. Several new solar array structures have been developed over the past 40 years to improve the array specific power and reduce the stowed volume during launch. The solar arrays presently in use can be classified into six categories: (1) body-mounted arrays; (2) rigid panel planar arrays; (3) flexible panel array; (4) flexible roll-out arrays; (5) concentrator arrays; and (6) high temperature/intensity arrays.

In addition, several proposed space missions have put other constraints on solar arrays. Several proposed Earth orbiting missions designed to study the Sun require “electrostatically clean” arrays. Inner planetary missions and mission to study the Sun within a few solar radii require solar arrays capable of withstanding temperatures above 450 °C and functioning at high solar intensities. Outer planetary missions require solar arrays that can function at low solar intensities and low temperatures. In addition to the near-Sun missions, missions to Jupiter and its moons also require solar arrays that can withstand high radiation levels (Ref. 1).

On Earth, the need for alternative energy is a high priority given the constant increase in worldwide population and despite recent advances in exploiting such resources, the fact that fossil fuel reserves are finite. For important applications involving terrestrial uses, price per watt will clearly be a critical driver. Conversely, the challenges of aerospace and defense have spurred the development of advanced technologies. Over the past half-century, researchers at the NASA Glenn Research Center (GRC) and their academic and industrial partners have

researched and developed a number of novel processing technologies, materials, devices, and energy conversion solutions for the challenges posed by surviving and even thriving in near-Earth space and non-terrestrial surface operations (Ref. 2).

We highlight several examples of advanced materials, processing and devices in this overview with examples of power technologies for space exploration and end with a discussion of their long-term potential for terrestrial applications. It is important to keep in mind the fact that solar cell materials and devices, regardless of the specific class of material(s) or device structure, are made to generate electricity or facilitate energy conversion processes. An important take-home lesson is that a wide array of power generation technologies exists, each technology with its unique ability to meet the difficulties posed by challenging mission power requirements (Ref. 3).

## 2.0 Inorganic Nanomaterials for Energy Conversion and Environmental Applications

The inclusion of nanocrystalline materials in photovoltaic devices has been proposed as a means to improve the efficiency of photon conversion (quantum dot solar cell) (Ref. 4), enable low-cost deposition of thin-films (Ref. 5), provide sites for exciton dissociation (Ref. 6), and pathways for electron transport (Ref. 7). With respect to their use in quantum dot solar cells and exciton dissociation, the size of the nanoparticle is an important factor in determining the optoelectronic properties of the material. When the size of a semiconductor quantum dot drops below that of the exciton Bohr radius (of the bulk material) the energy levels become quantized and the bandgap increases as the particle size decreases. In this size regime the bandgap can be “tuned” to a desired energy by adjusting the particle size. Quantum dots are also expected to be resistant to degradation from electron, proton, and alpha particle radiation, a requirement for use in space solar cells (Refs. 8 to 10). However, new generation solar cells based on nanostructured materials promise to enhance light harvesting efficiencies, greatly increasing their utility for future energy needs.

### 2.1 CuInE<sub>2</sub> (E = S, Se) and Related Nanomaterials From Single-Source Precursors

The chalcopyrite semiconductors copper indium disulfide (CuInS<sub>2</sub>) or diselenide (CuInSe<sub>2</sub>) have seen steady improvements in efficiency for thin-film photovoltaics. The bandgap of CuInS<sub>2</sub> ( $E_g = 1.5$  eV) is a good match to the AM0 solar spectrum, and CuInSe<sub>2</sub> ( $E_g = 1.1$  eV) is a promising low-cost electro-optical material (Ref. 11). Thin-film Cu(In,Ga)S<sub>2</sub> cells

with efficiencies of 12.8 percent have been successfully produced (Ref. 12), while Cu(In,Ga)Se<sub>2</sub> cells have been recorded with over 20 percent efficiency (Ref. 13). Earlier work in producing quantum dots of I-III-VI<sub>2</sub> materials relied on reactions involving CuInS<sub>2</sub> or CuInSe<sub>2</sub> nanoparticles from the chlorides and trioctylphosphine oxide (TOPO) (Ref. 14), treatment of a Cu<sup>I</sup>-P(OPh)<sub>3</sub>/In<sup>III</sup>-P(OPh)<sub>3</sub> mixture in acetonitrile with (TMS)<sub>2</sub>S (Ref. 15), or treatment of an aqueous mixture of CuCl and In<sub>2</sub>(SO<sub>4</sub>)<sub>3</sub> with hydrogen sulfide or hydrogen selenide, respectively (Ref. 16).

Controlled synthesis of a desired size nanoparticle is not always simple, especially for the higher-order ternary and tertiary materials. If separate sources are used for the different metals and chalcogenides, binary materials are often preferentially formed as a result of the different solubility of the products and reactivity of the precursors. A promising method to circumvent the formation of undesirable reaction products researched at GRC involved the use of single-source precursors. Single-source precursors are small molecules that include all the elements required in the final material. These precursors can be designed with many properties in mind including stoichiometry, solubility, and volatility.

A simple molecular precursor (PPh<sub>3</sub>)<sub>2</sub>CuIn(SET)<sub>4</sub> (1) (Figure 12) was first described by Prof. M. Kanatzidis's group (Ref. 17). This neutral complex comprises a copper(I) ion bound by two triphenylphosphine ligands, an indium(III) ion with two terminal ethanethiolate ligands, and two bridging ethanethiolate ligands between the metal centers. This molecule was found to decompose to produce CuInS<sub>2</sub> powders as depicted in Figure 1. Further work with this class of molecules has yielded analogous precursors with desirable properties such as lower melting points (including the liquid precursor (P<sup>n</sup>Bu<sub>3</sub>)<sub>2</sub>CuIn(SET)<sub>4</sub>) and higher solubility in organic solvents (Refs. 18 to 20). Note that this molecular structure is quite "tunable" and affords the ability to substitute for any of the ternary (Group 11, Group 13, or Group 16) elements in the I-III-VI<sub>2</sub> formula, as shown in Figure 2.

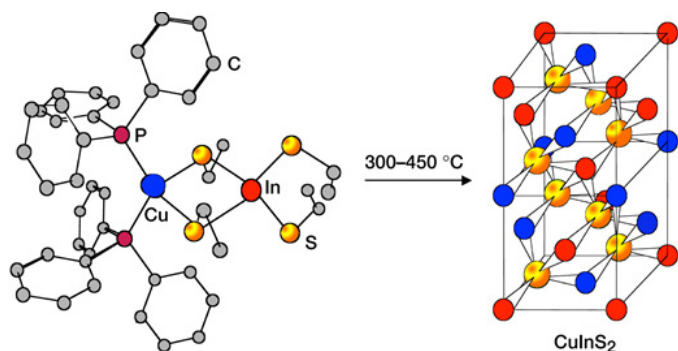


Figure 1.—Diagram of pyrolysis of [(PPh<sub>3</sub>)<sub>2</sub>Cu(SET)<sub>2</sub>In(SET)<sub>2</sub>] precursor (1) to produce semiconducting CuInS<sub>2</sub>.

We briefly describe work with the precursors for the synthesis of CuInS<sub>2</sub> or CuInSe<sub>2</sub> nanoparticles (Refs. 21 and 22). The reactions are outlined in Figure 3. The stepwise method of synthesis, isolating the red intermediates, is required for the purest products. If the precursor is brought directly to 250 or 300 °C, the final black powder is predominantly CuInS<sub>2</sub>, but impurity peaks are evident in the XRD pattern. X-ray powder diffraction patterns (Figure 4) clearly show that pure CuInS<sub>2</sub> is the product of the reaction at 250 and 300 °C, and CuInSe<sub>2</sub> at 275 and 300 °C. The powder diffraction patterns of the red powders from the 200 °C reactions exhibit unusual splitting of the (112) peaks into two peaks centered about the expected (112) position; the remaining two peaks (204/220) and (116/312) are in their expected positions. In all powder patterns, significant broadening of the diffraction lines is apparent; particle sizes of

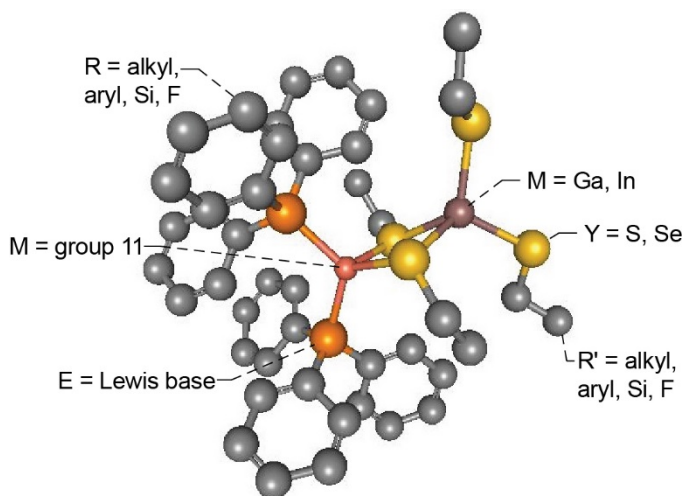
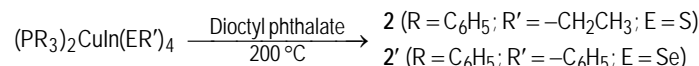


Figure 2.—Tunable sites for [(R<sub>3</sub>E)<sub>2</sub>M(QR')<sub>2</sub>M'(QR')<sub>2</sub>] architecture using [(PPh<sub>3</sub>)<sub>2</sub>Cu(SET)<sub>2</sub>In(SET)<sub>2</sub>] as an example.

### Synthesis of nanocrystalline CuInS<sub>2</sub> and CuInSe<sub>2</sub> from single-source precursors



2 and 2' are red-brown powders. Each is washed with toluene and methanol to remove unreacted precursor, dried under vacuum, and stored in a glove box for future use.



Figure 3.—Reaction scheme for the conversion of the single-source precursors to CuInS<sub>2</sub> or CuInSe<sub>2</sub>.

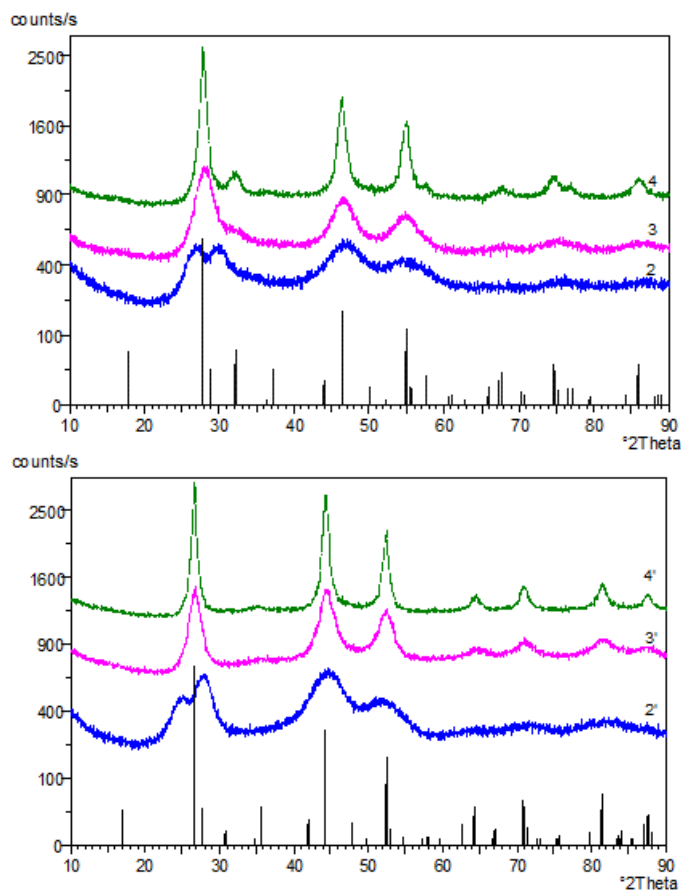


Figure 4.—Powder XRD patterns for a) 2, 3, and 4, the reaction products of  $[(\text{PPh}_3)_2\text{Cu}(\text{SEt})_2\text{In}(\text{SEt})_2]$  at 200, 250, and 300 °C, and b) 2', 3', and 4', the reaction products of  $[(\text{PPh}_3)_2\text{Cu}(\text{SeEt})_2\text{In}(\text{SeEt})_2]$  at 200, 275, and 300 °C.

2.1, 2.8 and 7.4 nm are calculated by the Scherrer formula for the 200, 250, and 300 °C  $\text{CuInS}_2$  powders, and 1.8, 4.4, and 9.8 nm for the 200, 275, and 300 °C  $\text{CuInSe}_2$  powders, respectively. The precise identity of the red-brown materials (2 for S and 2' for Se) has not been determined.

The powders were examined by transmission electron microscopy (TEM); typical TEM images are shown in Figure 5. Large particles seen (left image) are in fact aggregates of nanoparticles. From the high-resolution TEM (HRTEM) images, it appears that the size distribution of the samples is quite large, therefore, the sizes calculated by the Scherrer formula from the x-ray diffraction data are to be taken as only approximate. In conclusion, decomposition of single-source precursors at moderate temperatures affords nanoparticles of  $\text{CuInS}_2$  and  $\text{CuInSe}_2$  in good yield. These materials have nanometer-sized dimensions and may find utility in hybrid thin film or quantum dot solar cells. Future work includes altering the surface of the nanoparticles to enable dispersion in solvents, narrowing of the size distributions, and controlling the quantum dot bandgap as a function of size. A further observation to make

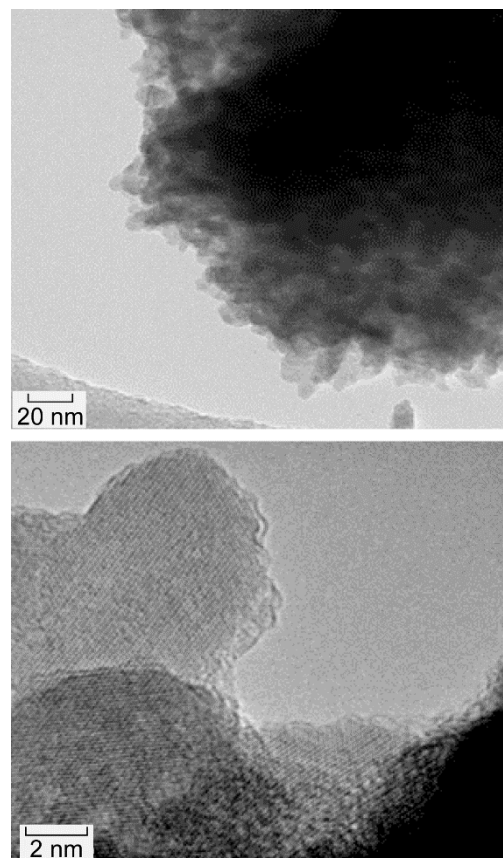


Figure 5.—Medium (top) and high-resolution (bottom) TEM images of sample 4' ( $\text{CuInSe}_2$ ).

is that this same approach utilizing single-source precursors and/or low-temperature processing can be used to produce quantum dots of the recently discovered perovskite solar cell materials that have shown much promise over the past several years (Ref. 23).

### 2.1.1 Low Temperature Growth of ZnO Nanorods Doped with Metals and Quantum Dots

In recent years, the wide-bandgap, semiconducting material zinc oxide (ZnO) has received significant attention; it has attractive electronic properties, it is relatively inexpensive, it is easy to prepare, and it is an environmentally friendly alternative to other semiconductors. As a result, it is used for a wide array of applications such as photovoltaics (Ref. 24), photoacoustic wave devices (Ref. 25), UV transceivers (Ref. 26), and photocatalysis (Ref. 27).

A method for manufacturing metal-doped ZnO nanostructured components of photovoltaic cells grown in solution at low temperature on a conductive indium tin oxide substrate (ITO) developed at the University of Tulsa (TU) is described. The growth of nanorods was achieved using a low-temperature, chemical bath deposition (CBD) procedure. Optimal growth

parameters were varied and tested with the goal of obtaining the greatest nanorod density, uniformity, and light absorption properties. Growth temperature, growth time, precursor concentration, cobalt dopant amount, and growth pH were each varied. Typically, ZnO based nanostructures and thin films absorb light in the UV region. By doping ZnO nanorods with cobalt and other metals, we can shift the absorption spectrum of ZnO from UV to the visible region. Arrays of ZnO nanorods can be templated using anodized aluminum oxide (AAO) membranes and then decorated with various semiconductor and metallic nanoparticles for comparison to doped and undoped ZnO thin films.

The CBD method (Ref. 28) developed at TU to incorporate metallic ions into ZnO structure holds great promise as a simple scalable, low temperature and cost effective method compared to pulsed laser deposition and chemical vapor deposition methods for fabricating ZnO nanorods and nanowires. In this method 1:1 ratio of 98 percent zinc nitrate hexahydrate ( $Zn(NO_3)_2 \cdot 6H_2O$ ) and hexamethylenetetramine were added to 125 mL of High Purity water, then placed in the oven at 95 °C for 24 h. Cobalt (II) nitrate hexahydrate, 98+ percent was incorporated into the solution before the hydrothermal process to dope at 5 percent. Finally, prepurchased cadmium selenide (CdSe) quantum dots in solution were dropped onto grown nanorods. In an attempt to increase efficiency, AAO membranes were sputter coated with 25 nm of Ag then adhered to ITO glass substrate using silver paste. The same growth procedure was followed as the non-spaced nanorods. SEM images were taken to verify growth of nanorods through the membrane pores. Once verified the membranes were dissolved in dilute NaOH leaving behind spaced and ordered nanorods. They could later be decorated with quantum dots (Ref. 29).

The synthesized ZnO nanorods grown via low temperature hydrothermal method are demonstrated in Figure 6. Experiments that contained Co doped nanorods were submitted to XRD and photoluminescence to assure absorption. ZnO nanorods with CdSe quantum dots are shown in Figure 6. The SEM image demonstrates a large amount of quantum dots that had adsorbed onto the surface. Photoluminescence was performed to demonstrate the shifting wavelength. The AAO membranes did space out the nanorods; however, the density of their growth is still lacking. Studies involving the impact of concentration and temperature adjustments are underway in order to demonstrate rational growth (Ref. 30).

## 2.2 Photocatalysis with Zinc Oxide Nanopowders

Particle size and shape influences the chemical, physical and electronic properties of the zinc oxide and its usefulness in the above-mentioned applications. As a result, many have investigated ways of controlling or modifying the size and

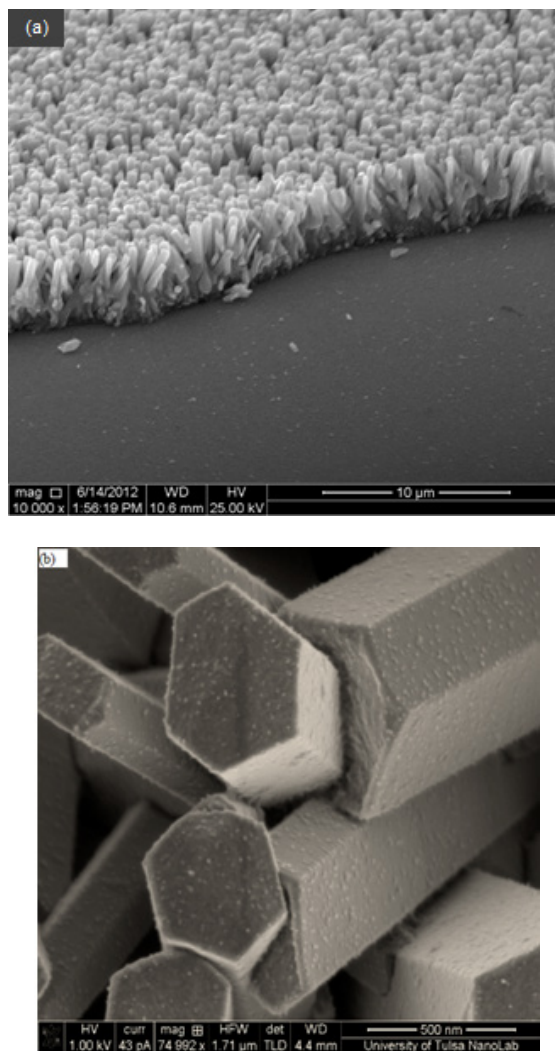
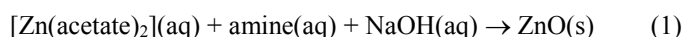


Figure 6.—(Top) SEM image of ZnO nanorods grown on ITO; (Bottom) SEM image of ZnO nanorods grown on ITO covered in CdSe Quantum dots.

morphology of ZnO particles by using different synthetic techniques, and modifying synthesis conditions (Refs. 31 to 34). The research group at Northwest Nazarene University (NNU) has been studying the bulk synthesis of zinc oxide nanoparticles and working to control both size and morphology of the nanoparticles prepared by sol-gel synthesis using  $[Zn(acetate)_2]$  in the presence of a variety of amines according to Equation (1) (Ref. 35).



The ZnO powders formed from the sol-gel process are then air dried and annealed in a nitrogen atmosphere at temperatures ranging from 150 to 300 °C for 2 h. X-ray powder diffraction confirmed formation of phase pure, wurtzite ZnO. X-ray pow-

der diffraction data for five samples prepared using five different amines are provided in Figure 7. All of the samples are phase pure and highly crystalline.

Although all of the samples are wurtzite ZnO, the presence of the different amines profoundly affects both the size and morphology of the resulting ZnO powders. Morphologies

produced include: spheres, rods, needles, plates, and small rice-shaped nanoparticles. Scanning electron microscope images of six of the powders are provided in Figure 8. Synthesis conditions also impact the size and shape of particles. In general, we have found that higher synthesis temperatures yield larger particles, and faster rates of NaOH addition yield smaller particles.

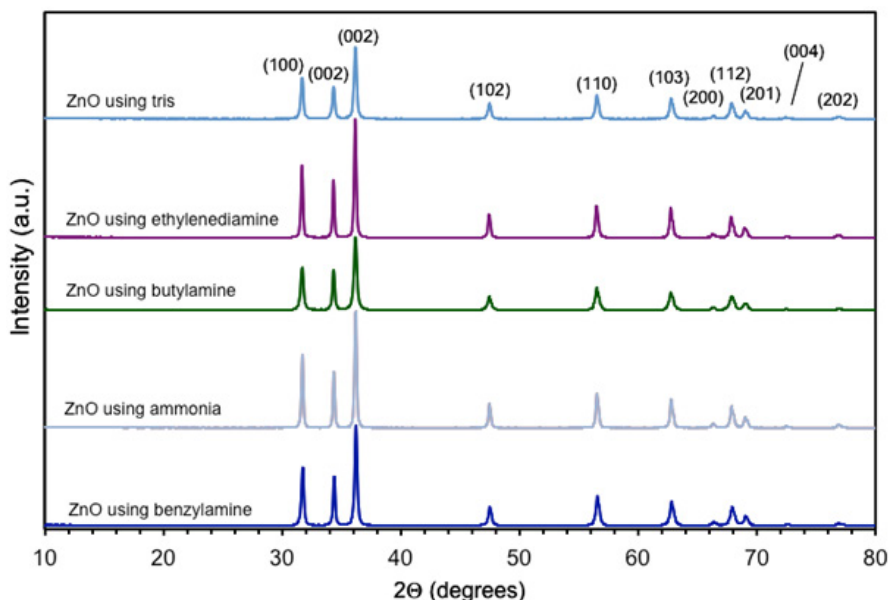


Figure 7.—Powder X-ray diffraction data for ZnO powders obtained by sol-gel synthesis at 75 °C using different amines. All products were annealed at 200 °C for 2 h in a nitrogen atmosphere.

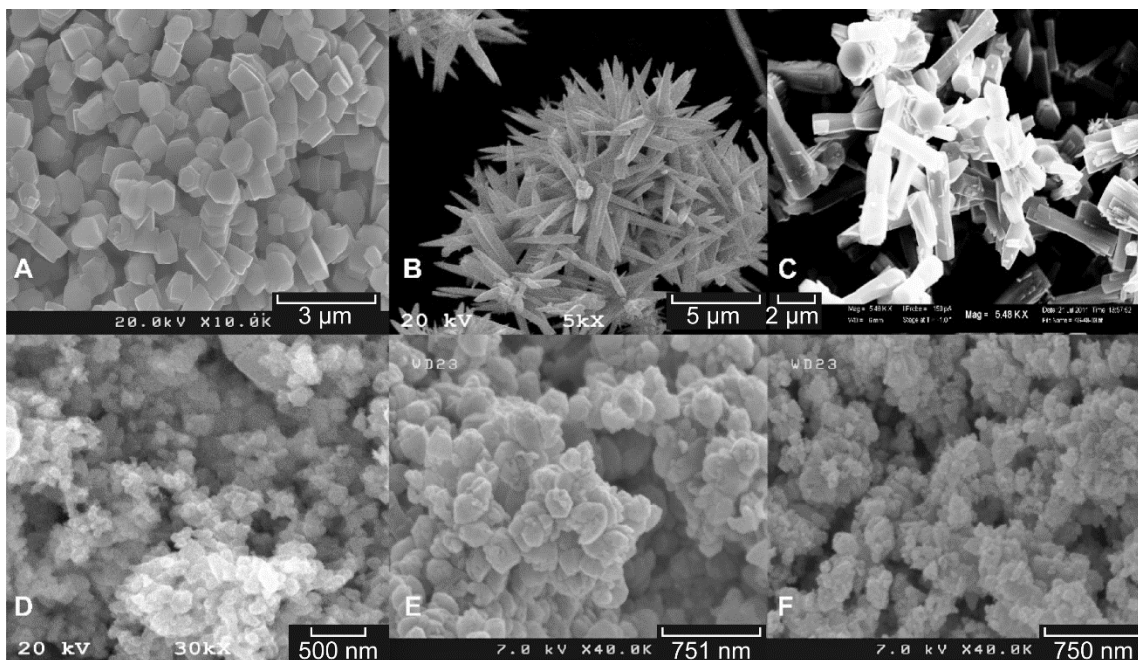


Figure 8.—SEM images of ZnO powders grown using different amines at different temperatures: (A) tris(hydroxymethyl)aminomethane (tris) at 95 °C, (B) ethylenediamine at 95 °C, (C) hydrazine at 95 °C, (D) t-butylamine at 95 °C, (E) triethanolamine at 65 °C, (F) 1,6-hexanediamine at 65 °C.

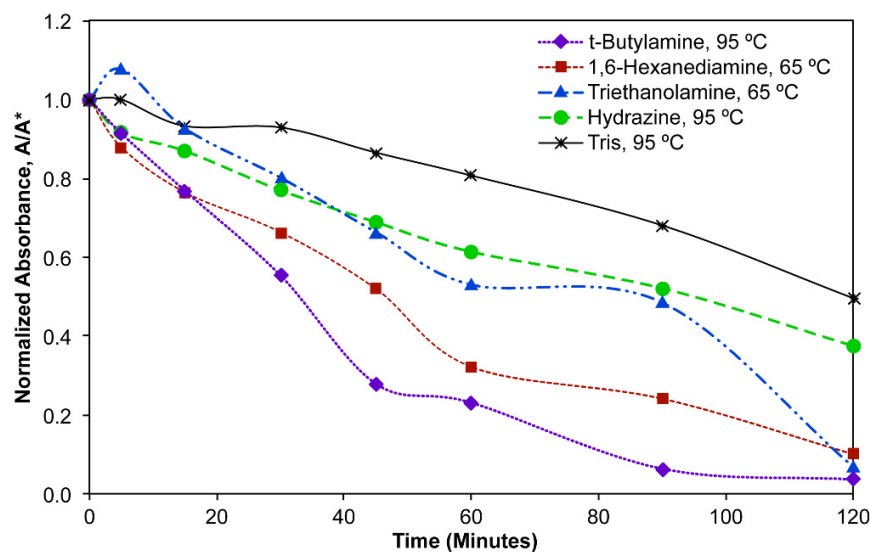


Figure 9.—Normalized absorbance at 558 nm versus time of ultraviolet irradiation (254 nm) of aqueous phenol red solutions in the presence of ZnO powders. The amine in the legend corresponds to the amine used in the synthesis of the ZnO.

The NNU research group has also been exploring the photochemical properties of the ZnO powders prepared using the different amines. We have found that the different size and morphologies of the powders influences the material's ability to catalyze photochemical reactions. For example, we have recently studied the different ZnO powders ability to photocatalyze the decomposition of the dye phenyl red under ultraviolet radiation. A summary of photocatalysis data for several of the powders is provided in Figure 9.

The plot is the normalized absorbance versus time for irradiation of phenol red solutions in the presence of ZnO powders prepared using four different amines. In general, it was found that smaller particles yielded faster decomposition rates than larger particles. Additionally, morphologies with a high surface area-to-volume ratio, such as rods or small, rice shaped crystals, also appear to increase the photocatalytic effectiveness. Therefore, by introducing different amines in the same synthetic protocol, we are able to modify both size and morphology of the prepared ZnO nanoparticles, and in turn impact ZnO's chemical reactivity.

### 3.0 Novel Production of Dye-Sensitized Solar Cells and Carbon Nanotubes

By the year 2050, the world's energy utilization will have doubled while fossil fuels utilization may continue to challenge our ability to exploit new sources. Fortunately, if just 0.2 percent of the Earth's surface were covered in 10 percent efficient solar cells by 2050, our energy needs would be met. The only significant barrier to such widespread deployment is cost. There are several third generation photovoltaics technologies that could make widespread solar cell deployment economically feasible.

Important technologies to enable advanced lightweight solar cells include dye-sensitized solar cells (DSSCs) (Ref. 7) and new carbon nanomaterials, such as carbon nanotubes (CNTs) (Ref. 36). These have both generated intense interest amongst scientists and engineers for fundamental insights into energy conversion and practical applications (Ref. 37). We outline several efforts geared towards advancing these technologies and enabling their inclusion in new, lightweight low-cost solar cells or other power devices for future dual-use applications.

#### 3.1 Efficient Inkjet Printed Dye Sensitized Solar Cells

With current DSSC efficiencies peaking at 13 percent (Ref. 38), the focus of research needs to shift to mass production. As DSSC are a relatively new technology that is constantly changing, any factories necessarily need to be flexible to remain competitive. Inkjet printing has the flexibility to accommodate materials changes and allows for the facile deposition of intricate patterns (Figure 10) without the expensive retooling and downtime associated with making new screens for screen-printing. To date, the group at University of Louisville (UofL) has printed DSSCs with efficiencies as high as 4.23 percent and can consistently produce 4 percent efficient DSSCs. While UofL's 4 percent efficient DSSCs are among the highest efficiency inkjet printed DSSCs in the world, there are still numerous gains to be made by optimizing the ink design and printing processes (Ref. 39).

The ink used by UofL to conduct their preliminary device fabrication trials and to develop printing strategies for the smooth nonporous substrates like fluorine-doped tin oxide (FTO) glass, conductive plastics, and stainless steel that are

likely to be used in industrial DSSC fabrications was unsuited for long term use and was determined to ultimately be the cause of the reduction in fill factor as seen in the IV curve of the nominally 15  $\mu\text{m}$  12 layer cell in Figure 10. This is due to a smaller than ideal titanium dioxide or titania ( $\text{TiO}_2$ ) nanoparticle size, uneven drying forcing the use of many thin layers and heat treatment cycles resulting in larger crystallite sizes and decreased porosity in the lower layers, and low overall porosity due to lack of a structure directing agent combined with the small particle size preventing dye absorption. To improve device efficiency and move towards industrially viable inks, our research has focused on developing  $\text{TiO}_2$  inks from the relatively inexpensive P25 nanopowder that are suitable for printing and designed to rectify the issues in the previous ink.

For an ink to be suitable for printing with the Dimatix DMP and related print heads, it must be stable for at least 24 h to

prevent particle agglomeration and nozzle clogging during printing, have a pH of 6-8 to prolong print-head life, have a surface tension in the 28 to 32  $\text{mN/m}^2$  range, a viscosity in the 6 to 12 cP range, good drop formation, deposit the suspended  $\text{TiO}_2$  as evenly as possible, and preferably use relatively non-toxic solvents. These requirements eliminated all of the traditional  $\text{TiO}_2$  colloidal dispersions due to their pH or use of large polymers. Two dispersions were produced with traditional bead milling techniques, a 5 wt%  $\text{TiO}_2$  1:2 1-butanol: cyclohexanol that was designed to air dry thin layers quickly and an extremely environmentally friendly 10 wt%  $\text{TiO}_2$  60:33:7 water:glycerol:1-butanol dispersion using 1 mM  $\text{Na}_4\text{P}_2\text{O}_7$  and 1 wt% ZetaSpere-1200 to improve dispersion stability. Initial tests of these dispersions indicate much better dye absorption than the previous inks (see Figure 11); UofL anticipates that efficiencies of cells made from these dispersions should improve accordingly.

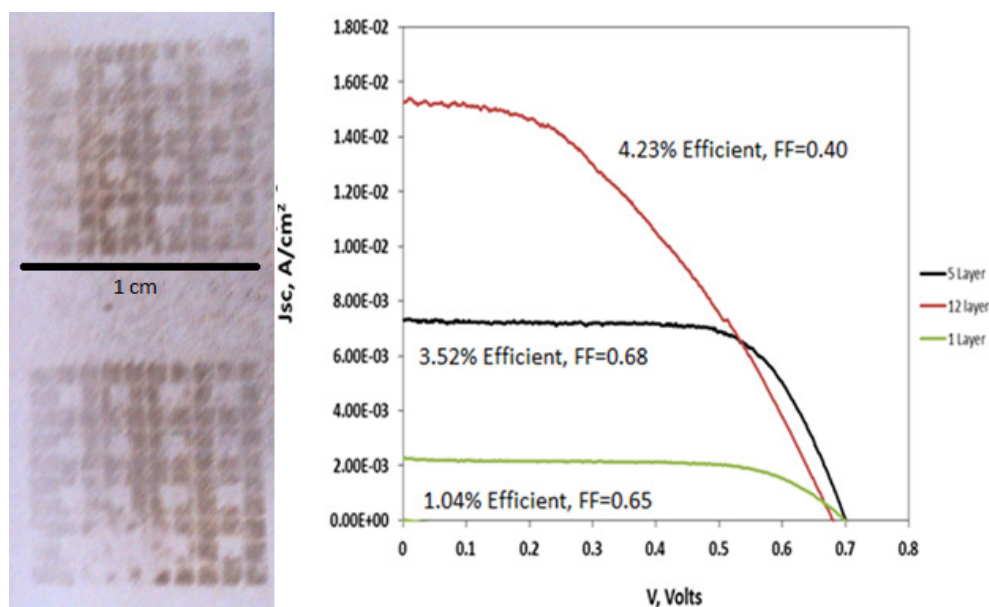


Figure 10.—(Left) Complex cell structure with sub 200  $\mu\text{m}$  grid lines printed with DMP2800 printer on  $\text{TiCl}_4$  treated,  $\text{O}_2$  plasma treated 316 Stainless Steel; (Right) IV curve of cells of increasing thickness printed from 10 wt%  $\text{TiO}_2$  2:1  $\text{H}_2\text{O}$ :glycerol ink with 1 percent Triton 100X.

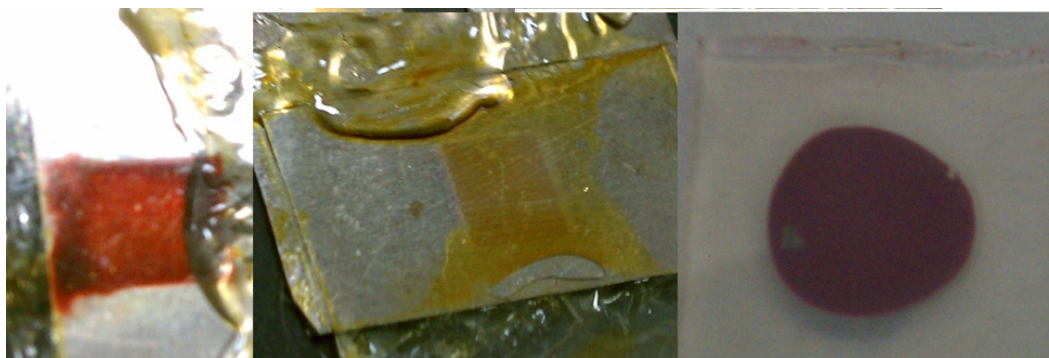


Figure 11.—Left to right: Dysol Paste; Old pH = 2 aqueous ink with 15 nm  $\text{TiO}_2$ ; new aqueous ink.

### 3.2 Iodide-Free Dye-Sensitized Solar Cells Using Nanowire-Based Architectures

In this study, the UofL group found that the performance of DSSCs can be improved by engineering the electron dynamics and surface properties of the semiconductor photoanode. We find that TiO<sub>2</sub> nanoparticles coated tin oxide nanowires yield DSSCs with ten times higher short-circuit current density than the widely employed TiO<sub>2</sub> nanoparticle, even when a commercially available ruthenium dye is used for sensitization. State of the art work in literature on improving the performance of DSCs using alternate redox electrolytes have only focused on using new organic dyes instead of the conventional Ru based dyes. Analysis of the literature data showed that Ru based dyes have higher reorganization energies compared to organic dyes and hence Ru based dyes are associated with high driving forces for dye-regeneration (Ref. 40). No attention has been paid to engineering the photoanode architecture for improving the performance with alternate redox electrolytes.

Prior studies using tin oxide nanowires in conjunction with iodide/triiodide redox electrolyte has shown that tin oxide nanowires have two orders of magnitude higher electron lifetimes and fast electron transport properties when compared to titania nanoparticles. In this study, the electron transport and recombination properties of different architectures involving nanoparticles, nanowires and nanoparticle/nanowire hybrid architectures of tin oxide and titania are compared to gain insight into the factors that contribute to the improved performance when alternate redox couples such as ferrocene/ferrocenium ( $\text{Fe}(\text{C}_5\text{H}_5)_2/\text{Fe}(\text{C}_5\text{H}_5)_2^+$ ) or heterocyclic (2,2,6,6-tetramethylpiperidin-1-yl)oxy and the cation species (TEMPO/TEMPO<sup>+</sup>) are used (Ref. 41).

The location of surface traps states and their passivation was found to have a significant impact the electron dynamics and photovoltaic characteristics of the DSC. The trap states in tin oxide nanowires are located very close to the conduction band (0.071 eV) when compared to titania nanoparticles that have much deeper trap states (0.24 eV). The shallow trap state in tin oxide nanowires allow faster detrapping of the electrons from the trap resulting in improvement of electron lifetimes over titania nanoparticles. In addition, the high diffusion lengths in tin oxide nanowires thicker photoanode films when alternate redox electrolytes are used thereby allowing increased sensitizer loading and light harvesting. Ongoing work is focused on new absorbers for achieving higher efficiencies (Figure 12).

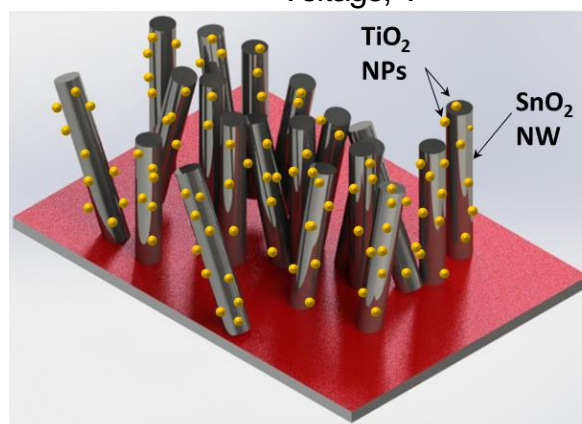
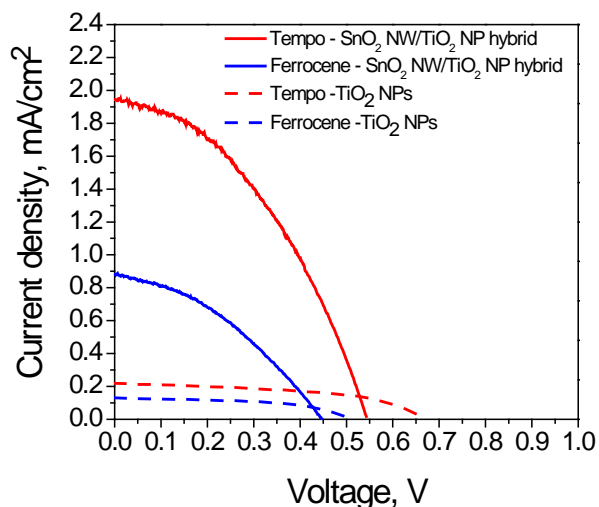


Figure 12.—(Top) Current-voltage characteristics of the TiO<sub>2</sub> NP/SnO<sub>2</sub> NW hybrid architecture and TiO<sub>2</sub> NP based DSCs with ferrocene and TEMPO redox electrolytes; (Bottom) SnO<sub>2</sub> NW/TiO<sub>2</sub> NP hybrid architectures.

### 3.3 Lower-Temperature Fabrication of Multiwalled Carbon Nanotubes

The unique mechanical and electronic properties of both single-walled and multiwalled varieties of carbon nanotubes have proven to be a rich source of new physics and have led to applications in a wide variety of materials and devices (Ref. 42). From an applications perspective, multiwalled carbon nanotube (MWNT) science and technology has developed rapidly since their discovery due to unique properties including high surface area, high mass-specific strength, controllable electronic properties, and thermal and chemical stability (Refs. 36, 37, and 42). Characteristic of MWNTs are the concentric graphene layers spaced 0.34 nm apart, with diameters from 10 to 200 nm and lengths up to hundreds of microns.

Carbon nanotubes (and recently graphene) are showing tremendous promise in improving the performance of power devices, such as thin film polymeric solar cells (Ref. 3) or electrochemically-based technologies (Ref. 36) such as direct-methanol fuel cells, lithium-ion ( $\text{Li}^+$ ) batteries, and ultracapacitors. In many of the power applications, the carbon nanotubes are used in concert with other materials often as a composite thin film (Ref. 3). Garnering control over the properties of both the carbon nanotubes and the resulting composites is an important step towards realizing device optimization.

Thus, a low-cost, simple MWNT production process is an important enabling technology. Preferential oriented MWNTs at

GRC were prepared by injection chemical vapor deposition (CVD) using an organometallic iron catalyst in toluene (see Figure 13) (Ref. 43). The concentration of the catalyst was found to influence both the growth (i.e., MWNT orientation) of the nanotubes, as well as the amount of iron in the deposited material (Ref. 36). Nanotubes were characterized by a variety of characterization techniques; as deposited, MWNTs contained as little as four weight percent of iron (Figure 14). This synthetic route provides a simple and scalable method to deposit MWNTs with a low defect density, low metal content and a preferred orientation (Figure 15) (Ref. 3).

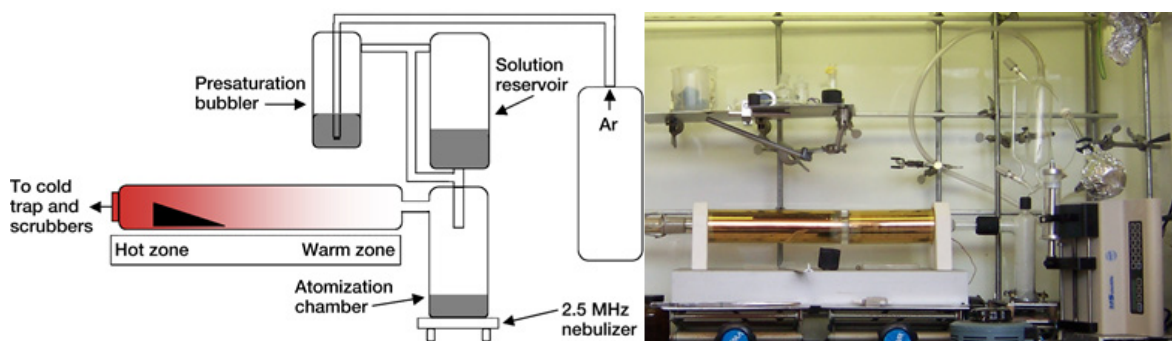


Figure 13.—Schematic (top) and picture (bottom) of an atmospheric-pressure hot-wall spray pyrolysis reactor.

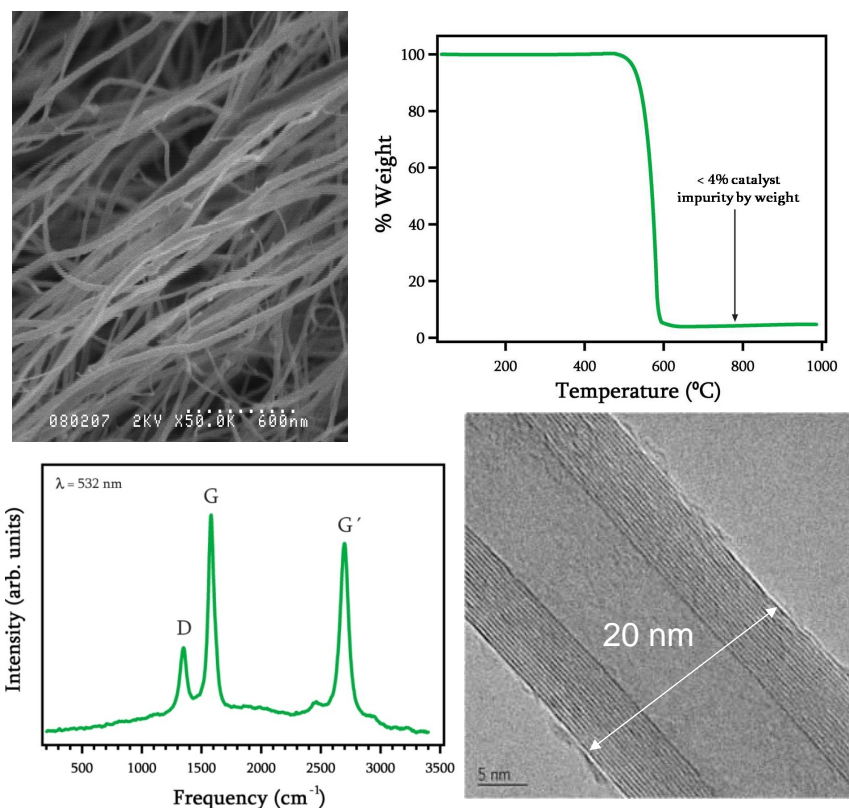


Figure 14.—Characterization data ensemble of MWNTs, clockwise from upper left: SEM, TGA, TEM, and Raman.

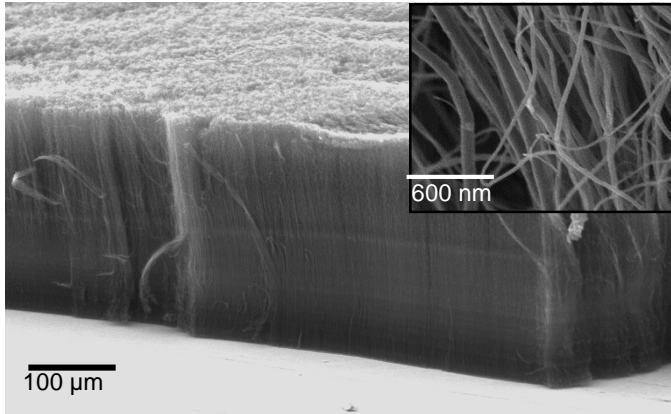


Figure 15.—Scanning electron micrograph of chemical vapor deposited multiwall carbon nanotube array on indium tin oxide coated glass. Inset: high-resolution micrograph of the multiwall carbon nanotubes.

## 4.0 Wide-Bandgap Semiconductor Materials for High-Power Devices

Silicon carbide (SiC) materials, processing, and device technologies occupy a critical space in wide bandgap semiconductors for harsh environments (Ref. 44). However, the poorly understood electrical influence of existing defects in SiC epitaxial layers is *the* bottleneck in the reliability of systems that use SiC devices. This lack of reliability has stymied the adoption of SiC devices by systems-integrators in industry, despite the various transformational systems level benefits they offer over silicon, such as higher speed, smaller payload, and higher efficiency. Work continues at and GRC (Ref. 45) and the University of South Carolina (USC) (Ref. 46) to improve prospects for SiC power devices and sensors, by gaining detailed physical insight into the statistical influence of defects, as was done with gallium nitride (GaN) technology for LED applications (Ref. 47), but remains unexplored with SiC.

### 4.1 State-of-the-Art SiC Homoepitaxy

The group at GRC has a long track record of developing various growth methods including CVD to grow several polytypes of SiC, particularly hexagonal materials, and to use these materials for the fabrication of various devices, including sensors, detectors, etc. (Ref. 48). One goal of processing hot wall chemical vapor deposition (HW-CVD) 4H-SiC using novel substrates is to dramatically reduce the concentration of defects to enable the fabrication of high-power devices. We briefly consider several relevant processing parameters (Table I) that are adjustable when growing SiC by HW-CVD, including: substrate type, growth temperature, chemical precursor(s) for Si and C, flow rate, pressure, composition of gases, and pre-/post-deposition treatment(s) (Refs. 49 to 52). Potential insights to be

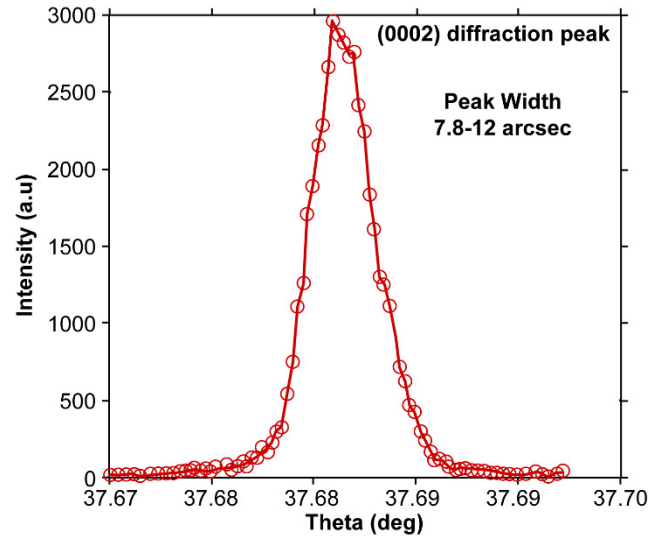


Figure 16.—X-ray rocking curve for a 60  $\mu\text{m}$  thick SiC epitaxial layer grown at USC, with FWHM < 10 arcsec.

gained from characterizing the resultant films are related to polytype(s), defect(s) and density, and measurable electrical parameters. As discussed below, the group at USC has had some success by employing halogen-containing precursors for reducing the defect density in 4H-SiC with improved subsequent device performance. The group at USC has demonstrated extremely high quality 4H-SiC homoepitaxy on  $8^\circ$  off-axis substrates at growth rates as high as  $108 \mu\text{m}/\text{h}$  using chlorine and transformational F-based chemistries (Refs. 52 and 53). The USC group has migrated to  $4^\circ$  and  $1^\circ$  substrates (Refs. 54 and 55). These high growth rates, essential for the commercialization of high voltage ( $> 10 \text{ kV}$ ) SiC power devices, have been obtained without sacrificing material quality. Surface morphologies are specular (Ref. 56), with doping concentrations  $< 10^{13} \text{ cm}^{-3}$  (Ref. 53), x-ray rocking curve widths  $< 10 \text{ arcsec}$  (Figure 16) and carrier lifetimes  $> 2 \mu\text{s}$ . Defect analysis reveals dislocation densities  $< 2000 \text{ cm}^{-2}$  being achieved routinely, comparable to, or better than, the state of the art in industry (Refs. 52 to 56), enabling the systematic defect isolation in small devices is described below. This capability was the result of Office of Naval Research (ONR) funded research at USC.

### 4.2 Etching and CVD Growth of 4H-SiC: Modeling of Surface/Small Molecule Interactions

To expedite development of low-defect 4H-SiC for high-power devices, it is critical to reduce the density of 3C-polytype growth-induced defects. While a vigorous HW-CVD growth effort is underway to utilize advanced substrate materials to produce such material, it is a time-consuming effort that could potentially be facilitated by getting some insights via first

TABLE I.—CVD PROCESSING PARAMETERS AND RESULTS RELEVANT TO (4H)-SiC GROWTH

| Substrate                                      | Conditions                                                                  | Precursor(s)                                                     | Results                                                                                                     | Issue(s)                                                                                                 | Reference |
|------------------------------------------------|-----------------------------------------------------------------------------|------------------------------------------------------------------|-------------------------------------------------------------------------------------------------------------|----------------------------------------------------------------------------------------------------------|-----------|
| 8° off-axis towards [11-20]                    | 140 torr, 1300 °C, C/Si = 6, H <sub>2</sub> = 8 slm (carrier gas)           | CH <sub>3</sub> Cl, SiCl <sub>4</sub>                            | At growth rates above 5 to 6 μm/h process window for good-quality low-temperature growth becomes too narrow | Triangular defects from formation of Si droplets in the gas phase                                        | 49        |
| 8° and 2° off-axis towards [11-20]             | 150 to 400 torr, 1300 to 1450 °C, C/Si and H <sub>2</sub> = variable        | CH <sub>3</sub> Cl, SiH <sub>4</sub> (3% in H <sub>2</sub> )     | E <sub>A</sub> = 0.57 eV for Si cluster formation/ evaporation                                              | Si cluster nucleation in the gas phase                                                                   | 50        |
| [0001] on-axis and 8° off-axis towards [11-20] | 50 to 250 torr, 1400 to 1850 °C, C/Si (variable) and H <sub>2</sub> = 5 slm | C <sub>3</sub> H <sub>8</sub> , SiCl <sub>4</sub>                | Growth-assisted etching was developed; hillock-like pits show distribution of micropipes                    | Mirror-like finish but over 1850 °C, uncontrolled etching                                                | 51        |
| [0001] 8° off-axis towards [11-20]             | 300 torr, 1550 °C, C/Si (0.9 to 1.7) and H <sub>2</sub> = 6 to 12 slm       | C <sub>3</sub> H <sub>8</sub> , SiH <sub>2</sub> Cl <sub>2</sub> | High growth rate (up to 100 μm/h) attained in chimney-type HW-CVD reactor                                   | No observable in-grown 3C-SiC inclusions or other morphological defects – eliminate Si cluster formation | 51        |

TABLE II.—EXAMPLES OF PRIOR FIRST PRINCIPLES STUDIES RELATED TO SILICON CARBIDE

| Topic studied                                                     | Method(s) used                                                                                                                                       | Conclusions                                                                                                                                                                                                                                      | Reference |
|-------------------------------------------------------------------|------------------------------------------------------------------------------------------------------------------------------------------------------|--------------------------------------------------------------------------------------------------------------------------------------------------------------------------------------------------------------------------------------------------|-----------|
| Energetics of the most common SiC polytypes                       | Density functional theory (DFT) on CASTEP with the PW91 generalized gradient approximation (GGA) functional together with ultrasoft pseudopotentials | Energy differences among SiC polytypes are enhanced at the surface with respect to the bulk                                                                                                                                                      | 57        |
| 4H-SiC(0001) and (000-1) surface processes at 1600 °C and 2300 °C | Combined Molecular dynamics (MD)/DFT calculations using CASTEP code                                                                                  | H abstraction reactions were slightly exothermic or endothermic with the order of energies: H < Br < Cl < F                                                                                                                                      | 58        |
| Substitutional impurity atoms in 4H-SiC                           | Plane-wave pseudopotential method implemented in Vienna ab initio simulation package (VASP) based on DFT                                             | Impurity atoms N, O, S substitute on C sites; B and Se depend upon the composition and growth conditions; all others (Be, Mg, Al, P, Zn, Ga, As, Cd, In, Sb, Te) substitute on Si sites                                                          | 59        |
| Electrically active defects of 4H-SiC                             | MD (Tersoff) and DFT with local-density approximation (LDA) implemented in VASP                                                                      | Native (or intrinsic) point defects of SiC are electrically active and have energy levels within the band gap of 4H-SiC. While it is possible to passivate Si vacancies using atomic hydrogen, C vacancies cannot be passivated in a similar way | 60        |

principles modeling studies. Several examples of prior activity by other groups and published in the literature are listed in Table II (Refs. 57 to 60).

When considering theoretical methods to facilitate determination of improved processing parameters for HW-CVD to produce low defect (< 10<sup>16</sup> defects/cm<sup>3</sup>) 4H-SiC, there are two approaches to consider: shareware/freeware or commercial packages. Below we provide a literature background, briefly mention some preliminary results on a related, relevant system and discuss potential directions moving forward. While Table II is certainly not an exhaustive list, it points to several areas of processing space that are potentially amenable to first principles modeling and subsequent analysis of SiC growth: polytype stabilities, surface processes, substitutional impurity, atom chemistry, and electrically active-defect formation.

As is clear from Table II, one approach for determining the most energetically stable configuration for atoms in a solid-state structural sense entails a combination of methods. Combining aspects of density functional theory (DFT) and Newtonian molecular dynamics (MD) will lend some insights into the most probable chemical species that exist on the surface and in

relevant more energetic domains in the bulk of the growing crystal. Commercial codes, while expensive, facilitate the combination of methods to address complex problems. Academic and/or freeware codes are inexpensive but often have minimal support or documentation; also combining methods requires transfer of data sets across software platforms with inherent complexities and inefficiencies.

An approach being employed at Florida A&M University (FAMU) involves numerically simulating a system using non-linear partial differential equations. A recent FAMU publication describes a novel modeling approach for an atomic layer deposition (ALD) process involving the first comprehensive numerical solution of the Dusty-Gas Model (DGM) and included a complete binary diffusion term (BDT) (Ref. 61). The purpose of this model was to predict the concentration of the reactant gases at the wafer. A one-dimensional model was constructed using mass conservation and dimensional analysis. FAMU introduced an explicit-implicit scheme to solve the DGM. After linearizing the equations, an implicit scheme (BDT) produced a program that solves the full DGM and is unconditionally stable (Ref. 61).

A concentration-dependent Damkohler number relevant to the purge step of the process was derived. The simulation matched the experimental data at a specific Damkohler number and further variation of the parameter confirmed existing experimentally observed phenomena (Ref. 61). Our current plan is to extend this model to two dimensions to simulate flow across and around a SiC substrate in a HW-CVD reactor. Insights from modeling reported in the literature will be utilized to inform our choice of parameters and interpretation of and correlation with experimental results.

### 4.3 SiC Device Fabrication and Characterization: Isolating or Reducing Impact of Defects

With lower defect epitaxy demonstrated (Figure 17), the group at USC is currently fabricating diodes using their demonstrated processes on material grown on various off-cuts of SiC; this would allow for isolating single defects in individual unipolar Schottky and bipolar p-i-n diodes. USC will focus on single and compound basal plane dislocations (BPD's), threading edge and screw dislocations (TED's, TSD's), step bunching, along with other important defects that may emerge (Figure 18) (Refs. 52 to 56, and 62 to 64).

While crystal growers typically attempt to eliminate all defects, this is not a tractable solution, as there are inevitably tradeoffs; i.e., basal plane dislocations vs. screw dislocations in SiC. However, if the electrical influence of the defects is known, crystal growers can tackle the more disruptive ones, while they can tolerate less severe defects. By correlating the electrical performance with the defect profile of devices in a statistical fashion, the electrical role of individual defects can

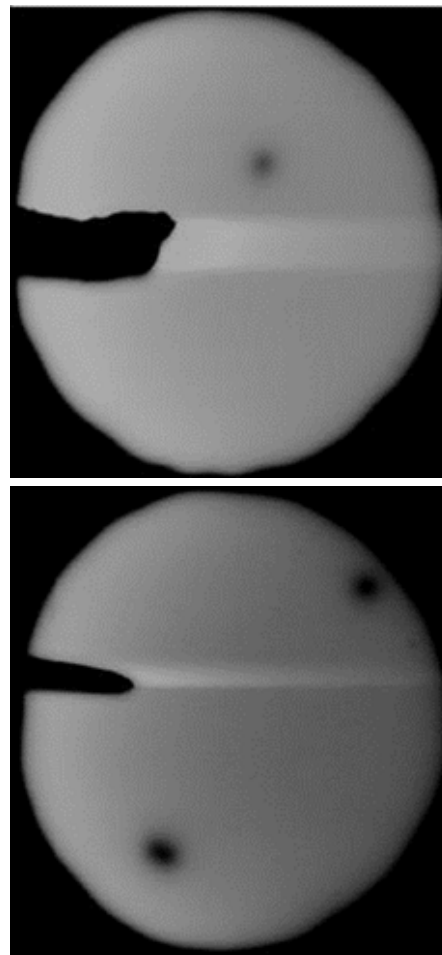


Figure 17.—Electron beam induced current-SEM images of Schottky diodes 70  $\mu\text{m}$  in diameter containing (top) single and (bottom) two defects in active region.

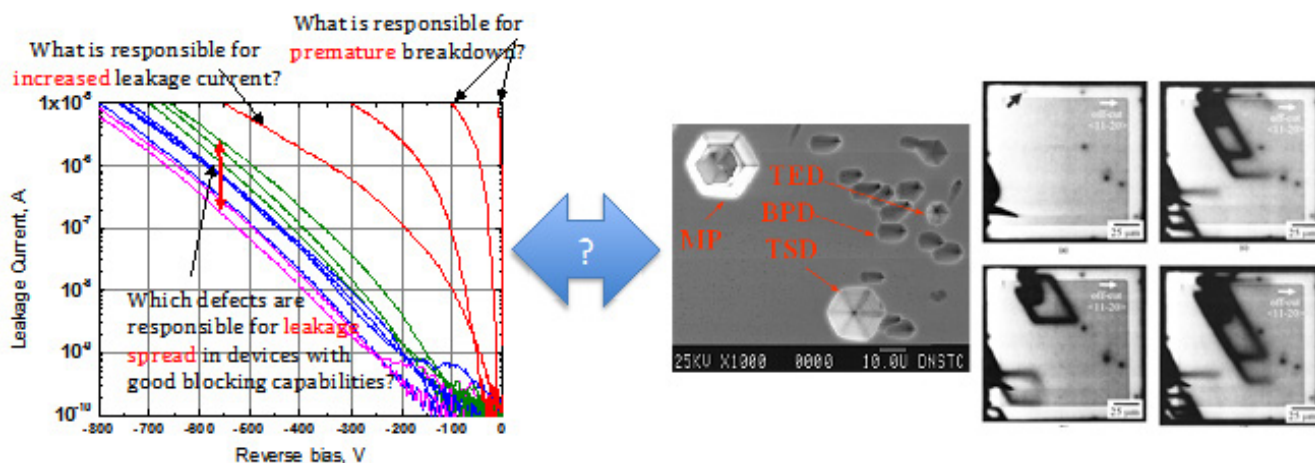


Figure 18.—(Left) Static reverse breakdown I-V curves of an ensemble of commercial Schottky diodes characterized at USC. The large scatter in the performance shows the clear influence of defects; (Middle) SEM of typical KOH etched defects in SiC epitaxial layers; (Right) Dynamic evolution of stacking faults from a BPD under  $200/\text{cm}^2$  stress in a SiC bipolar pin diode at USC. The systematic connection between these factors has never been investigated and represents the key bottleneck to SiC device adoption by systems integrators.

be isolated. Post-deposition etching is one approach to “managing” acceptable defect levels to improve device performance.

Finally, besides use of modeling to improve quality of grown materials, it is feasible to model device performance analytically and with physics-based finite element tools to understand the physical origin of defects and their influence on device performance. Alternatively, it is certainly reasonable to propose developing physics-based circuit models for devices with multiple defects, to be incorporated into larger systems level simulations. These models will be tested on large devices with multiple defects to be able to “reverse-engineer” the defect profile of a given device based on its electrical characteristics. As noted above, the next generation of SiC devices has great potential for dual-use applications in diverse fields such as biomedicine, aerospace and defense, engines, and energy. The next section continues this theme for several other promising processing, materials and device technologies.

## 5.0 Dual-Use Applications of Novel Processing, Materials, and Devices

We begin this section with several intriguing applications of photovoltaics for space exploration in two quite different size regimes that speak to the need for numerous solutions to the problems posed by the need to provide reliable power. An innovative approach to intelligent systems design is the subject of the second subsection that describes the concept, design, and

testing of an integrated power device in low Earth orbit (LEO). The essence of dual-use applications is the ability to repurpose technology designed to withstand the rigors and challenge of the space environment for terrestrial situations that present similar problems and issues, though perhaps not in a simultaneous fashion. Another important aspect of the GRC effort that should certainly not be overlooked is the variety of individual collaborations fostered, organizational partnerships formed, and students educated and brought into the aerospace community as a result of the technical work. The final section gives an explicit example of an educational tool derived from a NASA-driven power material need and solution.

### 5.1 Space Exploration and Science Enabled by Advanced Materials and Devices

An obvious application for advanced high performance photovoltaics technology is to enable interplanetary travel in the solar system via solar electric propulsion (SEP); solar arrays provide the power for various electric propulsion engines. For example, NASA’s Dawn spacecraft combines innovative state-of-the-art technologies pioneered by other recent missions with commercial and repurposed components (Ref. 65). With its solar array in the retracted position (for launch), the Dawn spacecraft is approximately 7 ft long; with its wide solar arrays extended, Dawn expands to a length of 65 ft (Figure 19). Dawn was launched in September 2007 and spent nearly 14 months orbiting Vesta, the second most massive object in the main



Figure 19.—This artist's concept shows NASA's Dawn spacecraft heading toward the dwarf planet Ceres. Dawn spent nearly 14 months orbiting Vesta, the second most massive object in the main asteroid belt between Mars and Jupiter, from 2011 to 2012. It is heading towards Ceres, the largest member of the asteroid belt. When Dawn arrives, in February 2015, it will be the first spacecraft to go into orbit around two destinations in our solar system beyond Earth. (NASA/JPL-Caltech)

asteroid belt between Mars and Jupiter, from 2011 to 2012. It is heading towards Ceres, the largest member of the asteroid belt. When Dawn arrives, in February 2015, it will be the first spacecraft to go into orbit around two destinations in our solar system beyond Earth.

On the other end of the spacecraft size spectrum are CubeSats, a class of small satellites that roughly fall into the “nanosatellite” regime. They are based upon a standard form factor of 10 cm (~4 in.) on a side. Thus a one-unit (1U) CubeSat has a volume of 1000 cm<sup>3</sup> or 1 liter. Other standard sizes include 2U (2x1U), 3U (3x1U), and 6U (3x2U). The sizes reflect standard delivery pods to launch CubeSats from a variety of platforms; 3U is currently the most typical CubeSat size. Currently for launch safety, the maximum mass guidance for a CubeSat is 1.33-2 kg/U. As a consequence of the reasonable (low) cost and opportunity for learning to be derived from participation in CubeSat missions, many CubeSats that have been designed, built, and flown are affiliated

with an institution of higher learning. An excellent recent and up-to-date review on the state of the art of small spacecraft technology, with an emphasis on CubeSats has been published by our colleagues at the NASA Ames Research Center and includes a significant amount of information on relevant technologies as well as the legacy of small satellite (~20 percent CubeSat) missions from the past 15 years (Ref. 66).

We recently developed a concept using a parametric spacecraft assessment study for a mission to a diminutive asteroid (DAVID) in the latter half of 2019, given an opportunity for inclusion of a 6U CubeSat on the Space Launch System Exploration Mission-1, currently projected for a December 17, 2017 launch. The core of the science payload for this proposed mission would be based upon advanced SiC radiation sensors enabled by the device development technologies described above. Figure 20 shows a diagram of the 6U CubeSat with a block system diagram as well as several candidate device architectures

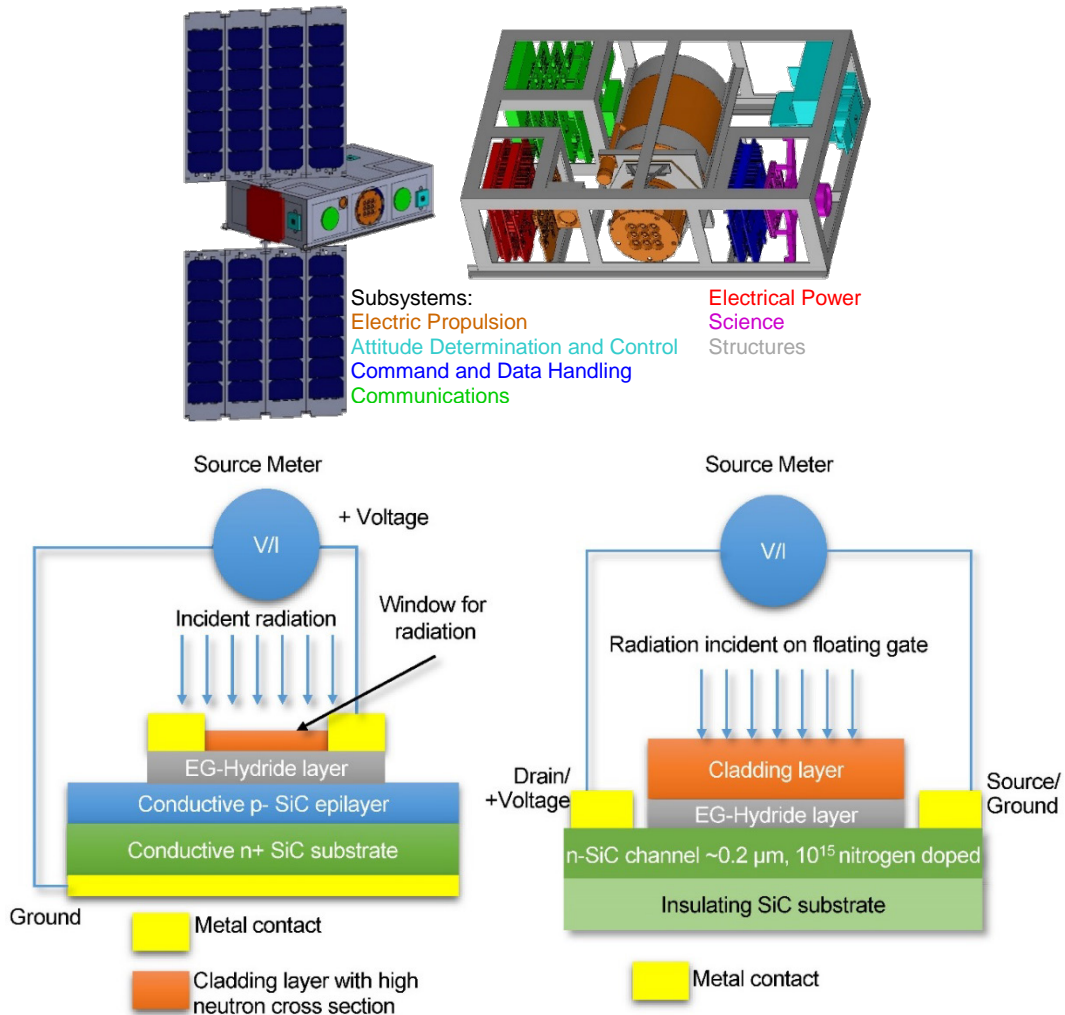


Figure 20.—(Top) Schematic and systems diagram of DAVID, a 6U CubeSat designed to rendezvous with an asteroid; (Bottom) Architectures of two SiC-based devices to provide radiation detection capabilities for instruments to be integrated into DAVID or other CubeSats.

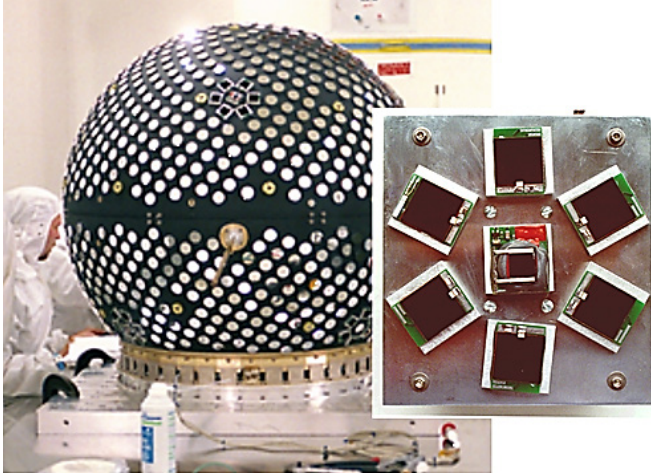


Figure 21.—Starshine 3 nanosatellite; inset: close-up of an IMPS surrounded by six commercial triple-junction III-V solar cells.

(Ref. 66). Finally, it is interesting to note that travel from a trans-lunar orbit to the destination asteroid is also provided by SEP technology, albeit much smaller than Dawn. To briefly summarize, the CubeSat format during the brief period of its development has demonstrated great value as an educational paradigm as well as an intriguing low-cost platform for advanced technology demonstration for LEO and beyond.

## 5.2 Integrated Power Technologies

GRC has been working to develop lightweight, integrated space power systems on small or flexible substrates. These systems generally consist of a high efficiency thin film solar cell, a high energy density solid-state lithium-ion battery, and the associated control electronics in a single monolithic package. These devices can be directly integrated into microelectronic or MEMS devices and are ideal for distributed power systems on satellites or even the main power supply on a nanosatellite (Ref. 68). These systems have the ability to produce constant power output throughout a varying or intermittent illumination schedule as would be experienced by a rotating satellite or “spinner” and by satellites in a LEO by combining both generation and storage. An integrated thin film power system has the potential to provide a low mass and cost alternative to the current SOA power systems for small spacecraft. Integrated thin film power supplies simplify spacecraft bus design and reduce losses incurred through energy transfer to and from conversion and storage devices. It is hoped that this simplification will also result in improved reliability.

GRC developed and flew an integrated microelectronic power supply (IMPS) for a space flight experiment in conjunction with the Project Starshine atmospheric research satellite (see Figure 21) (Ref. 69). This device integrates a seven

junction small-area GaAs monolithically integrated photovoltaic module (MIM) with an all-polymer  $\text{LiNi}_{0.8}\text{Co}_{0.2}\text{O}_2$  lithium-ion thin film battery. The array output is matched to provide the necessary 4.2 V charging voltage and minimized the associated control electronic components. The use of the matched MIM and thin film Li-ion battery storage maximizes the specific power and minimizes the necessary area and thickness of this microelectronic device. This power supply was designed to be surface mounted to the Starshine 3 satellite, was ejected into a LEO with a fixed rotational velocity of  $5^\circ$  per second after launch from Kodiak, Alaska, on September 30, 2001. The satellite de-orbited on January 21, 2003, after 7,434 revolutions around the Earth. The IMPS successfully provided continuous power even with the intermittent illumination due to the satellite rotation and LEO. Data from the 2 weeks of testing indicated that the Sun-facing supply maintained a voltage in the range of 2.8 to 2.9 V from initial reading of 2.65 V; for IMPS charged mainly by Earth’s albedo, the comparable readings were a range of 2.55 to 2.65 V from initial reading of 2.5 V.

Finally, as power-integrated (or integrated-power) devices and systems are designed, fabricated, and successfully tested, utilization across a range of applications can be anticipated. A typical method for technology transfer involves patenting and licensing new inventions and handing off inventions to the private sector for further development. An example of intellectual property (IP) resulting from a collaboration on a solar cell/battery device with an industry and a not-for-profit entity (Ref. 70). The resulting patent issued several years ago is owned by Aerospace Corporation and is currently under negotiation for licensing by the private sector. Other examples of technology transfer are discussed in the following section.

## 5.3 Technology Transfer to Facilitate Nanotechnology Research and Education

As discussed in several examples above, advanced (nano)materials, processing, and the devices that they enable have numerous potential dual-use applications. The multiyear effort on developing and utilizing single-source precursors for I-III-VI<sub>2</sub> thin film- and nanomaterials produced significant IP that was patented and is currently jointly owned by GRC and the Ohio Aerospace Institute (OAI) (Ref. 71). Several companies have negotiated a license for the technology but at this time, no agreement has been reached. An earlier example of a related technology resulted in the formation of a small business. CVD-deposited gallium sulfide passivates gallium arsenide (GaAs) and improves the performance of several classes of GaAs devices (Refs. 72 and 73) Gallia, Inc. was formed in Weston, Massachusetts, to commercialize this technology (Refs. 74 and 75). After several years of operation, TriQuint Semiconductor ([www.triquint.com](http://www.triquint.com)) of Hillsboro, Oregon, purchased



Figure 22.—Nanotech Innovations LLC's commercially available MWNT production reactor, SSP-354.

Gallia, Inc., and all rights to the technology. It is anticipated that NASA will eventually utilize these technologies in commercial off-the-shelf (COTS) products.

Because GRC was more interested in the power technologies that could result from the incorporation of carbon nanotubes, and not in the actual production of the carbon nanotubes themselves, the Center released the IP to the inventors in 2005 (Ref. 43). Subsequently, this technology has been transferred to Nanotech Innovations LLC (NTI) in Oberlin, Ohio (Ref. 76). For several years, the company had focused on improving the device. In 2010, NTI was awarded a patent for the process and apparatus to grow high quality, low-impurity carbon nanotubes. A portable, bench-top system, called the SSP-354 (Figure 22), can make research-scale quantities of high quality nanotubes within just a few hours. A major advantage of the NASA-derived technology is that it is a single-step process; the user simply loads the injector and presses start. Currently, the machine is supporting the incorporation of carbon nanotubes into education curricula, research, and product-development endeavors for small-scale applications (Ref. 77).

## 6.0 Conclusions: Lessons Learned and (Other) Terrestrial Applications

On Earth, the need for alternative energy is a high priority given the constant increase in worldwide population and despite recent advances in exploiting such resources, the fact that fossil fuel reserves are finite. For important applications involving terrestrial uses, price per watt will clearly be a critical driver. Conversely, the challenges of aerospace and defense have spurred the development of advanced technologies. These

challenges can be addressed by a variety of technologies that overcome issues involving available area, efficiency, reliability, and specific power at an optimal cost. The particular application may be in aerospace, defense, utility, consumer, grid-based, off-grid, recreational, or industrial settings. Organic-based photovoltaics will most likely provide solutions in applications where price and/or large area challenges dominate such as consumer or recreational products. Inorganic materials will most likely predominate in aerospace and defense uses: satellites, non-terrestrial surface power, and planetary exploration.

The inclusion of nanocrystalline materials in photovoltaic devices has been proposed as a means to improve the efficiency of photon conversion (quantum dot solar cell), enable low-cost deposition of thin-films, provide sites for exciton dissociation, and pathways for electron transport. A promising method to circumvent the formation of undesirable reaction products involves the use of single-source precursors, small molecules that include all the elements required in the final material. These precursors can be designed with many properties in mind including stoichiometry, solubility, and volatility. The wide-bandgap, semiconducting material ZnO has received significant attention recently due its many outstanding properties; it is used for a wide array of applications including photovoltaics and photocatalysis. The performance of DSSCs can be improved by engineering the electron dynamics and surface properties of the semiconductor photoanode. From an applications perspective, MWNT science and technology has developed rapidly since their discovery due to unique properties including controllable electronic properties and stability. New generation solar cells based on nanostructured materials promise to enhance light harvesting efficiencies, greatly increasing their utility for future energy needs.

The poorly understood electrical influence of existing defects in SiC epitaxial layers is a critical bottleneck in the reliability of systems that use SiC devices. This lack of reliability has stymied the adoption of SiC devices by systems-integrators in industry, despite the various transformational systems level benefits they offer over silicon, such as higher speed, smaller payload, and higher efficiency. The next generation of SiC devices has great potential for dual-use applications in diverse fields such as biomedicine, aerospace and defense, engines, and energy.

Advanced high performance photovoltaics technology enables interplanetary travel in the solar system (i.e., NASA's Dawn spacecraft) via SEP; solar arrays provide the power for various electric propulsion engines. For example, combines innovative state-of-the-art technologies pioneered by other recent missions with commercial and repurposed components. On the nanosatellite (spacecraft) end of the scale, the CubeSat format during the brief period of its development has demonstrated great value as an educational paradigm as well as an intriguing

low-cost platform for advanced technology demonstration for LEO and beyond.

An integrated thin film power system has the potential to provide a low mass and cost alternative to the current SOA power systems for small spacecraft. Integrated thin film power supplies simplify spacecraft bus design and reduce losses incurred through energy transfer to and from conversion and storage devices. It is hoped that this simplification will also result in improved reliability. As power-integrated (and other advanced) devices and systems are designed, fabricated, and successfully tested, utilization across a range of applications can be anticipated. A typical method for technology transfer involves patenting and licensing new inventions and handing off inventions to the private sector for further development. Other more creative partnerships and collaborations will at times be necessary to break down institutional barriers.

The essence of dual-use applications is the ability to repurpose technology designed to withstand the rigors and challenge of the space environment for terrestrial situations that present similar problems and issues, though perhaps not in a simultaneous fashion. An important aspect of the GRC effort that should certainly not be overlooked is the variety of individual collaborations fostered, organizational partnerships formed, and students educated and brought into the aerospace community as a result of the technical work.

## References

1. Bailey, S.G., and Flood, D.J., "Space Photovoltaics," *Prog. Photovolt. Res. Appl.*, Vol. 6, No. 1, pp. 1-14, 1998.
2. Hepp, A.F., Bailey, S.G., and Raffaele, R.P., "Inorganic Photovoltaic Materials and Devices: Past, Present, and Future," *Organic Photovoltaics: Mechanisms, Materials and Devices*, S.-S. Sun and N.S. Sariciftci, eds., CRC Press, Boca Raton, FL, pp. 19-36, 2005.
3. Hepp, A.F., McNatt, J.S., Bailey, S.G., Raffaele, R.P., Landi, B.J., Sun, S.-S., Bonner, C.E., Banger, K.K., and Rauh, D., "Ultra-Lightweight Space Power from Hybrid Thin-Film Solar Cells," *IEEE Aerospace and Elec. Systems*, Vol. 23, No. 9, pp. 31-41, 2009.
4. Luque, A., and Martí, A., "Increasing the Efficiency of Ideal Solar Cells by Photon Induced Transitions at Intermediate Levels," *Phys. Rev. Lett.*, Vol. 78, No. 26, pp. 5014-5017, 1997.
5. Eberspacher, C., Pauls, K., and Serra, J., "Non-Vacuum Processing of CIGS Solar Cells," Proceedings of the 29<sup>th</sup> IEEE Photovoltaics Specialist Conference, Institute of Electrical and Electronic Engineers, Piscataway, NJ, pp. 684-687, 2002.
6. Huynh, W.U., Dittmer, J.J., and Alivisatos, A.P., "Hybrid Nanorod-Polymer Solar Cells," *Science*, Vol. 295, No. 5564, pp. 2425-2428, 2002.
7. Grätzel, M., "Perspectives for Dye-Sensitized Nanocrystalline Solar Cells," *Prog. Photovolt.*, Vol. 8, No. 1, pp. 171-185, 2000.
8. Marcinkevičius, S., Leon, R., Čechavičius, B., Siegert, J., Lobo, C., Magness, B., and Taylor, W., "Changes in Carrier Dynamics Induced by Proton Irradiation in Quantum Dots," *Physica B*, Vol. 314, Nos. 1-4, pp. 203-206, 2002.
9. Walters R.J., Summers, G.P., Messenger, S.R., Freundlich, A., Monier, C., and Newman, F., "Radiation Hard Multi-Quantum Well InP/InAsP. Solar Cells for Space Applications," *Prog. Photovolt.*, Vol. 8, No. 3, pp. 349-354, 2000.
10. Sobolev, N.A., Cavaco, A., Carmo, M.C., Grundmann, M., Heinrichsdorff, F., and Bimberg, D., "Enhanced Radiation Hardness of InAs/GaAs Quantum Dot Structures," *Phys. Stat. Sol B*, Vol. 224, No. 1, pp. 93-96, 2001.
11. Contreras, M.A., Egaas, B., Ramanathan, K., Hiltner, J., Swartzlander, A., Hasoon, F., and Noufi, R., "Progress Toward 20% Efficiency in Cu(In,Ga)Se<sub>2</sub> Polycrystalline Thin-Film Solar Cells," *Prog. Photovolt.*, Vol. 7, No. 4, pp. 311-316, 1999.
12. Klenk, R., Klaer, J., Köble, Ch., Mainz, R., Merdes, S., Rodriguez-Alvarez, H., Scheer, R., and Schock H.W., "Development of CuInS<sub>2</sub>-Based Solar Cells and Modules" *Sol. Energy Mater. Sol. Cells*, Vol. 95, No. 6, pp. 1441-1445, 2011.
13. Chirilă, A., Reinhard, P., Pianezzi, F., Bloesch, P., Uhl, A.R., Fella, C., Kranz, L., Keller, D., Gretener, C., Hagerdorfer, H., Jaeger, D., Erni, R., Nishiwaki, S., Buecheler, S., and Tiwari, A.N., "Potassium-Induced Surface Modification of Cu(In,Ga)Se<sub>2</sub> Thin Films for High-efficiency Solar Cells," *Nature Materials*, Vol. 12, No. 12, pp. 1107-1111, 2013.
14. Malik, M.A.; O'Brien, P. and Revaprasadu, N., "A Novel Route for the Preparation of CuSe and CuInSe<sub>2</sub> Nanoparticles," *Adv. Mater.*, Vol. 11, No. 17, pp. 1441-1444, 1999.
15. Czekelius, C., Hilgendorff, M., Spanhel, L., Bedja, I., Lerch, M., Müller, G., Bloeck, U., Su, D.-S., and Giersig, M., "A Simple Colloidal Route to Nanocrystalline ZnO/CuInS<sub>2</sub> Bilayers," *Adv. Mater.*, Vol. 11, No. 8, pp. 643-646, 1999.
16. Gurin, V.S., "Nanoparticles of Ternary Semiconductors in Colloids: Low-Temperature Formation and Quantum Size Effects," *Coll. Surf. A*, Vol. 142, No. 1, pp. 35-40, 1998.
17. Hirpo, W., Dhingra, S., Sutorik, A.C., and Kanatzidis, M.G., "Synthesis of Mixed Copper-Indium Chalcogenolates. Single-Source Precursors for the Photovoltaic Materials CuInQ<sub>2</sub> (Q = S, Se)," *J. Am. Chem. Soc.*, Vol. 115, No. 4, pp.1597-1599, 1993.

18. Banger, K.K., Cowen, J., and Hepp, A.F., "Synthesis and Characterization of the First Liquid Single-Source Precursors for the Deposition of Ternary Chalcopyrite (CuInS<sub>2</sub>) Thin Film Materials," *Chem. Mater.*, Vol. 13, No. 11, pp. 3827-3829, 2001.
19. Banger, K.K., Hollingsworth, J.A., Harris, J.D., Cowen, J., Buhro, W.E., and Hepp, A.F., "Ternary Single-Source Precursors for Polycrystalline Thin-Film Solar Cells," *Appl. Organomet. Chem.*, Vol. 16, No. 11, pp. 617-627, 2002.
20. Banger, K.K., Jin, M.H.-C., Harris, J.D., Fanwick P.E., and Hepp, A.F., "A New Facile Route for the Preparation of Single-Source Precursors for Bulk, Thin-Film, and Nanocrystallite I-III-VI Semiconductors," *Inorg. Chem.*, Vol. 42, No. 24, pp. 7713-7715, 2003.
21. Castro, S.L., Bailey, S.G., Raffaele, R.P., Banger, K.K., and Hepp, A.F., "Nanocrystalline Chalcopyrite Materials (CuInS<sub>2</sub> and CuInSe<sub>2</sub>) via Low-Temperature Pyrolysis of Molecular Single-Source Precursors," *Chem. Mater.*, Vol. 15, No. 8, pp. 3142-3147, 2003.
22. Castro, S.L., Bailey, S.G., Raffaele, R.P., Banger, K.K., and Hepp, A.F., "Synthesis and Characterization of Colloidal CuInS<sub>2</sub> Nanoparticles from a Molecular Single-Source Precursor," *J. Phys. Chem. B*, Vol. 108, No. 33, pp. 12429-12435, 2004.
23. Boix, P.P., Nonomura, K., Mathews, N., and Mhaisalkar, S.G., "Current Progress and Future Perspectives for Organic/Inorganic Perovskite Solar Cells," *Materials Today*, Vol. 17, No. 1, pp. 16-23.
24. Ennaoui, A., Weber, M., Scheer, R., and Lewerenz, H.J., "Chemical-Bath ZnO Buffer Layer for CuInS<sub>2</sub> Thin-Film Solar Cells," *Sol. Energy Mater. Sol. Cells*, Vol. 54, No. 1, pp. 277-286, 1998.
25. Lee, J.B., Lee, H.J., Seo, S.H., and Park, J.S., "Characterization of Undoped and Cu-doped ZnO Films for Surface Acoustic Wave Applications," *Thin Solid Films*, Vols. 398-399, pp. 641-646, 2001.
26. Look, D.C., Reynolds, D.C., Litton, C.W., Jones, R.L., Eason, D.B., and Cantwell, G., "Characterization of Homoepitaxial p-Type ZnO Grown by Molecular Beam Epitaxy," *Appl. Phys. Lett.*, Vol. 81, No. 10, pp. 1830-1832, 2002.
27. Udom, I., Ram, M.K., Stefanakos, E.K., Hepp, A.F., and Goswami, D.Y., "One Dimensional-ZnO Nanostructures: Synthesis, Properties and Environmental Applications," *Mater. Sci. Semicond. Process.*, Vol. 16, No. 6, pp. 2100-2114, 2013.
28. Hari, P., Seay, J., Farmer, K., and Roberts, K.P., "Cobalt Doped ZnO Nanorods Fabricated by Chemical Bath Deposition Technique," *Advances in Science and Technology*, Vol. 77, pp. 280-284, 2012.
29. Hari, P. and Spencer, D., "Surface Morphology of Zinc Oxide Nanorods Grown by Hydrothermal Deposition Technique," *Physica Status Solidi C*, Vol. 6, No. S1, pp. S150-S153, 2009.
30. Hari, P., Farmer, K., and Roberts, K.P., "pH Study of Zinc Oxide Nanorods Grown on Indium Tin Oxide Coated Substrate," *Canadian J. of Physics*, published online Oct. 2013, doi: 10.1139/cjp-2013-0616, 2013.
31. Zhou, H. and Li, Z., "Synthesis of Nanowires, Nanorods and Nanoparticles of ZnO Through Modulating the Ratio of Water to Methanol by Using a Mild and Simple Solution Method," *Mater. Chem. Phys.*, Vol. 89, Nos. 2-3, pp. 326-331, 2005.
32. Wang, B.G., Shi E.W., and Zhong, W.Z., "Understanding and Controlling the Morphology of ZnO Crystallites under Hydrothermal Conditions," *Cryst. Res. Technol.*, Vol. 32, No. 5, 2006, pp. 659-667.
33. Xu, Z.Z., Ben, Y., Chen, Z.L., and Qi, F., "Facile synthesis of snowflake-like ZnO nanostructures at low temperature and their super catalytic activity for the ozone decomposition," *Mater. Res. Bull.*, Vol. 48, No. 4, pp. 1725-1727, 2013.
34. Meagley K. L. and Garcia, S. P., "Chemical Control of Crystal Growth with Multidentate Carboxylate Ligands: Effect of Ligand Denticity on Zinc Oxide Crystal Shape," *Cryst. Growth Des.*, Vol. 12, No. 2, 2012, pp. 707-713.
35. Hays, J., Thurber, A., Reddy, K.M., Punnoose, A., and Engelhard, M.H., "Development and Processing Temperature Dependence of Ferromagnetism in Zn<sub>0.98</sub>Co<sub>0.02</sub>O," *J. Appl. Phys.*, Vol. 99, No. 8, pp. 08M123.1-08M123.3, 2006.
36. Iijima, S., "Helical Microtubules of Graphitic Carbon," *Nature*, Vol. 354, No. 6348, pp. 56-58, 1991.
37. Raffaele, R.P., Landi, B.J., Harris, J.D., Bailey, S.G., and Hepp, A.F., "Carbon nanotubes for power applications," *Mater. Sci. Eng. B*, Vol. 116, No. 3, pp. 233-243, 2005.
38. Grätzel, M. et al., "Dye-Sensitized Solar Cells with 13% Efficiency Achieved through the Molecular Engineering of Porphyrin Sensitizers," *Nature Chem.*, Vol. 6, No. 3, pp. 242-247, 2014.
39. Kuscer, D., Stavber, G., Trefalt, G., and Kosec, M., "Formulation of an Aqueous Titania Suspension and Its Patterning with Ink-Jet Printing Technology," *J. Amer. Ceram. Soc.*, Vol. 95, No. 2, pp. 487-493, 2012.
40. Robertson, N. et al., "Varying Numbers and Positions of Carboxylate Groups on Ru Dyes for Dye-Sensitized Solar Cells: Uptake on TiO<sub>2</sub>, Cell Performance and Cell Stability," *RSC Advances*, Vol. 4, No. 20, pp. 10165-10175, 2014.
41. Chu, T.C. et al., "Ionic Liquid with a Dual-Redox Couple for Efficient Dye-Sensitized Solar Cells," *Chem. Sus. Chem.*, Vol. 7, No. 1, pp. 146-153, 2014.

42. Dai, H., "Carbon nanotubes: opportunities and challenges," *Surf. Sci.*, Vol. 500, Nos. 1-3, pp. 218–241, 2002.
43. Harris, J.D., Raffaele, R.P., Gennett, T., Landi, B.J., and Hepp, A.F., "Growth of Multi-Walled Carbon Nanotubes by Injection CVD Using Cyclopentadienyliron Dicarbonyl Dimer and Cyclooctatetraene Iron Tricarbonyl," *Mater. Sci. Eng. B*, Vol. 116, No. 3, pp. 369-374, 2005.
44. Wijesundara, M.B.J. and Azevedo, R.G., *Silicon Carbide Microsystems for Harsh Environments*, NY: Springer, 2011.
45. Neudeck, P.G., Steven L. Garverick, S.L., Spry, D.J., Chen, L.-Y., Beheim, G.M., Krasowski, M.J., and Mehregany, M., "Extreme Temperature 6H-SiC JFET Integrated Circuit Technology," *Phys. Stat. Sol. A*, Vol. 206, No. 10, pp. 2329-2345, 2009.
46. Omar, S.U., Sudarshan, T.S., Rana, T.A., Song H., and Chandrashekhar, M.V.S., "Large Barrier, Highly Uniform and Reproducible Ni-Si/4H-SiC Forward Schottky Diode Characteristics: Testing the Limits of Tung's Model," *J. Phys. D: Appl. Phys.*, Vol. 47, No. 29, pp. 295102.1-295102.9, 2014.
47. Nakamura, S. and Krames, M.R., "History of Gallium-Nitride-Based Light-Emitting Diodes for Illumination," *Proc. IEEE*, Vol. 101, No. 10, pp. 2211-2220.
48. Neudeck, P.G., "Silicon Carbide Technology," Chapter 5, *The VLSI Handbook*, ed., W.-K. Chen, CRC Press, 2<sup>nd</sup> Ed., Boca Raton, FL, pp. 5.1-5.34, 2007.
49. Kotamraju, S., Krishnan, B., Melnychuk, G., and Koshka, Y., "Low-Temperature Homoepitaxial Growth of 4H-SiC with CH<sub>3</sub>Cl and SiCl<sub>4</sub> Precursors," *J. Cryst. Growth*, Vol. 312, No. 5, pp. 645-650, 2010.
50. Koshka, Y., Lin, H.-D., Melnychuk, G., and Wood, C., "Epitaxial Growth of 4H-SiC at Low Temperatures Using CH<sub>3</sub>Cl Carbon Gas Precursor: Growth Rate, Surface Morphology, and Influence of Gas Phase Nucleation," *J. Cryst. Growth*, Vol. 294, No 2, pp. 260-267, 2006.
51. Dhanaraj, G., Dudley, M., Chen, Y., Ragothamachar, B., Wu, B., and Zhang, H., "Epitaxial Growth and Characterization of Silicon Carbide Films," *J. Cryst. Growth*, Vol. 287, No. 2, pp. 344-348, 2006.
52. Chowdhury, I., Chandrashekhar, M.V.S., Klein, P.B., Caldwell, J.D., and Sudarshan, T., "High Growth Rate 4H-SiC Epitaxial Growth using Dichlorosilane in a Hot-Wall CVD Reactor," *J. Cryst. Growth*, Vol. 316, No. 1, pp. 60-66, 2011.
53. Chandrashekhar, M.V.S., Chowdhury, I., Kaminski, P., Kozlowski, R., Klein, P.B., and Sudarshan, T., "High Purity Semi-Insulating 4H-SiC Epitaxial Layers by Defect-Competition Epitaxy: Controlling Si Vacancies," *Appl. Phys. Expr.*, Vol. 5, No. 2, pp. 025502.1-025502.3, 2012.
54. Rana, T.A., Song H., Chandrashekhar, M.V.S., and Sudarshan, T.S., "Comparison of 4H Silicon Carbide Epitaxial Growths at Various Growth Pressures Using Dichlorosilane and Silane Gases," *Mat. Sci. Forum*, Vols. 717-720, pp. 117-120, 2012.
55. Omar, S.U., Chandrashekhar, M.V.S., Chowdhury, I., Rana, T.A., and Sudarshan, T.S., "Step Dynamics in the Homoepitaxial Growth of 6H-SiC by Chemical Vapor Deposition on 1° Offcut Substrate using Dichlorosilane as Si Precursor," *J. Appl. Phys.*, Vol. 113, No. 18, pp. 184904.1-184904.8, 2013.
56. Rana, T.A., Song H., Chandrashekhar, M.V.S., and Sudarshan, T.S., "Behavior of Particles in the Growth Reactor and Their Effect on Silicon Carbide Epitaxial Growth," *Mat. Sci. Forum*, Vols. 717-720, pp. 153-156, 2012.
57. Mercier, F. and Nishizawa, S., "Role of Surface Effects on Silicon Carbide Polytype Stability," *J. Cryst. Growth*, Vol. 360, No. 1, pp. 189-192, 2012.
58. Olander, J. and Larsson, K.M.E., "An *Ab Initio* Study of 4H-SiC(0001) and (000-1) Surface Processes at Experimental Temperatures," *Thin Solid Films*, Vol. 458, Nos. 1-2, pp. 191-196, 2004.
59. Miyata, M., Higashiguchi, Y., and Hayafuji, Y., "Ab Initio Study of Substitutional Impurity Atoms in 4H-SiC," *J. Appl. Phys.*, Vol. 104, No. 12, pp. 123702.1-123702.5, 2008.
60. Chatterjee, A., Bhat, A., and Matocha, K., "Investigation of Electrically Active Defects of Silicon Carbide Using Atomistic Scale Modeling and Simulation," *Physica B*, Vols. 401-402, pp. 81-84, 2007.
61. Jones III, A.-A.D. and Jones, Jr. A.D., "Numerical Simulation and Verification of Gas Transport During an Atomic Layer Deposition Process," *Mater. Sci. Semicond. Process.*, Vol. 21, No. 1, pp. 82-90, 2014.
62. Grekov, A., Zhang, Q., Fatima, H., Agarwal, A., and Sudarshan, T.S., "Effect of Crystallographic Defects on the Reverse Performance of 4H-SiC JBS Diodes," *Microelec. Reliab.*, Vol. 48, No. 10, pp. 1664-1668, 2008.
63. Muzykov, P.G., Kennedy, R.M., Zhang, Q., Capell, C., Burk, A., Agarwal, A., and Sudarshan, T.S., "Physical Phenomena Affecting Performance and Reliability of 4H-SiC Bipolar Junction Transistors," *Microelec. Reliab.*, Vol. 49, No. 1, pp. 32-37, 2009.
64. Maximenko, S.I., Pirouz, P., and Sudarshan, T.S., "Investigation of the Electrical Activity of Partial Dislocations in SiC p-i-n Diodes," *Appl. Phys. Lett.*, Vol. 87, No. 3, pp. 033503.1-033503.3, 2005.
65. Dawn Mission Page, [http://www.nasa.gov/mision\\_pages/dawn/main/index.html](http://www.nasa.gov/mision_pages/dawn/main/index.html), Sept. 30, 2013.
66. Mission Design Division Staff, "Small Spacecraft Technology State of the Art," NASA/TP—2014-216648, 2014.
67. Landis, G.A., Colozza, A.J., Hepp, A.F., Stegeman, J.D., Oleson, S.R., COMPASS Team, and Chandrashekhar, M.V.S., "Diminutive Asteroid Visitor using Ion Drive (DAVID): A Detailed 6U-CubeSat Mission Analysis of a

- Near Earth Asteroid Visit Done at NASA GRC,” *Small Sat-28 Conference Proceedings*, Paper SSC14-XI-7, 2014.
68. Raffaele, R.P., Hepp, A.F., Landis, G.A., and Hoffman, D.J., “Mission Applicability Assessment of Integrated Power Components and Systems,” *Progress in Photovoltaics*, Vol. 10, No. 6, pp. 391-397, 2002.
  69. Wilt, D.M., Hepp, A.F., Moran, M., Jenkins, P.P., Scheiman, D.A., and Raffaele, R.P., “Integrated Micro-Power System (IMPS) Development at NASA Glenn Research Center,” *Proc. Internat. Micropower and Microdev. Symp.*, Vol. 2002-25, Electrochemical Society, Inc., Pennington, NJ, pp. 194-202, 2003.
  70. Simburger, E.J., Matsumoto, J.H., Gierow, P.A., and Hepp, A.F., “Integrated Thin Film Battery and Circuit Module,” *United States Patent*, No. 7,045,246, 2006.
  71. Banger, K.K., Hepp, A.F., Harris, J.D., Jin, M.H., and Castro, S.L., “Single-Source Precursors for Ternary Chalcopyrite Materials, and Methods of Making and Using the Same,” *United States Patent*, No. 6,992,202, 2006.
  72. Power, M.B., MacInnes, A.N., Jenkins, P.P., Barron, A.R., and Hepp, A.F., “Enhancement of Photoluminescence Intensity of GaAs with Cubic GaS Chemical Vapor Deposited Using a Structurally Designed Single-Source Precursor,” *Appl. Phys. Lett.*, Vol. 62, No. 7, pp. 711-713, 1993.
  73. Tabib-Azar, M., Kang, S., MacInnes, A.N., Power, M.B., Barron, A.R., Jenkins, P.P., and Hepp, A.F., “Electronic Passivation of *n*- and *p*-type GaAs Using Chemical Vapor Deposited GaS,” *Appl. Phys. Lett.*, Vol. 63, No. 5, pp. 625-627, 1993.
  74. Barron, A.R., Jenkins, P.P., MacInnes, A.N., and Hepp, A.F., “Metal, Passivating Layer, Semiconductor, Field-Effect Transistor,” *United States Patent*, No. 5,760,462, 1998.
  75. Barron, A. R., Jenkins, P. P., MacInnes, A. N., and Hepp, A. F., “Minority Carrier Device Comprising a Passivating Layer Including a Group 13 Element and a Chalcogenide Component,” *United States Patent*, No. 6,008,525, 1999.
  76. Hepp, A. F. and Harris, J. D., “Process and Apparatus Utilizing Mixed Ligand Organometallic Catalysts for In Situ Growth of High Purity, Low Defect Density Carbon Nanotubes,” *United States Patent*, No. 7,763,230 B2, 2010.
  77. Flood, D.M., Flood, D.J., Harris, J.D., and Hepp, A.F., “Nanotube Production Devices Expand Research Capabilities,” *Spinoff 2011*, Ed.-in-Chief, B. Schwerin, NP-2011-11-780-HQ, pp. 148-149, 2012.





